Chapter 3
Modes

Antoine Chaigne and Jean Kergomard

Abstract The concept of mode (or eigenmode) is ubiquitousin musical acoustics, since the behavior of musical instruments, as many other mechanical systems, is fairly described by boundary value models, for which the modes are the eigensolutions, in the strict mathematical sense. In this chapter, the basic properties of the eigenmodes are reviewed, for both discrete and continuous non dissipative systems. The efficiency of the modal description is illustrated by numerous examples taken from the physics of strings and percussive instruments. In addition, most of the results presented in this chapter will be used in Chap. 7 devoted to wind instruments. It is shown, in particular, to what extent the geometry, material, and conditions of excitation determine the vibrational properties of the instruments. Fundamental results on the vibrations of strings, beams, membranes, plates, and shells are demonstrated, which will be used throughout the book. The links with experimental modal analysis are also emphasized.

3.1 Introduction

The concept of *modes* is widely used in musical acoustics. Experimentally, one can gain a visual appreciation of modes through the so-called *Chladni patterns* (see Fig. 3.1). Such patterns are obtained by sprinkling sand on a plane or on a slightly curved structure (plate and soundboard) which is being continuously excited (using, for example, a bow, or a loudspeaker driven by a sinusoidal input signal).[1]

[1]Chladni patterns on drumheads were obtained by Worland [43].

A. Chaigne (✉)
Institute of Music Acoustics, University of Music and Performing Arts Vienna (MDW), Anton-von-Webern-Platz 1, 1030 Vienna, Austria
e-mail: antchaigne@gmail.com

J. Kergomard
CNRS Laboratoire de Mecanique et d'Acoustique (LMA), 4 impasse Nikola Tesla CS 40006, 13453 Marseille Cedex 13, France
e-mail: kergomard@lma.cnrs-mrs.fr

A. Chaigne, J. Kergomard, *Acoustics of Musical Instruments*, Modern Acoustics and Signal Processing, DOI 10.1007/978-1-4939-3679-3_3

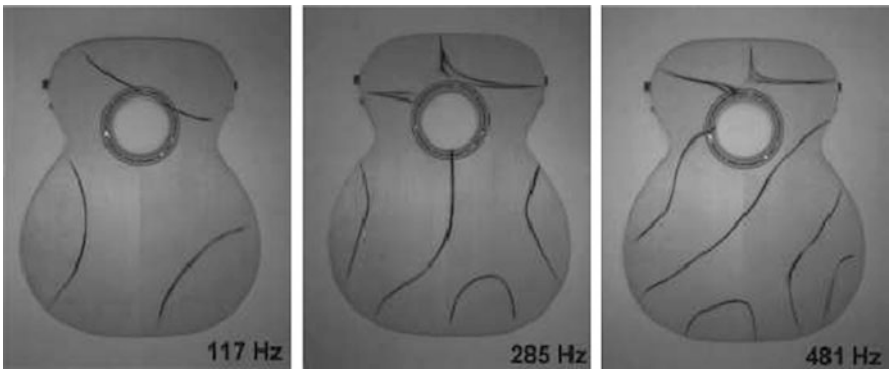

Fig. 3.1 Chladni patterns showing the modes of vibration of a guitar soundboard, at 117, 285 and 481 Hz, respectively. According to [41]. © Thomas Erndl

It is observed that the grains gather together on continuous lines, or nodal lines, corresponding to points with zero amplitude of vibration. The resulting figure is the *mode shape* corresponding to the excited *eigenfrequency*. One can clearly hear the associated sound when the structure is weakly damped, as it is the case for a metallic plate. In what follows, *eigenmodes*, or simply *modes*, designate the set of eigenfrequencies and mode shapes of a continuous, or of a discrete, system for a given geometry and material.

In the previously described experiment, different modes can be successively excited if the excitation point, or the excitation frequency, is modified. If the boundary conditions are changed, then the eigenmodes and eigenfrequencies also change. This result has important consequences in lutherie: it shows that the violin soundboard, once glued to the instrument, does not exhibit the same eigenmodes as it did when it was free to vibrate at the edge.

From a theoretical point of view, the concept of modes is of great interest. Because of their mathematical orthogonality, it is possible to expand any linear solution of vibratory or acoustic phenomena onto a basis of eigenmodes. In Chap. 8, it will be shown under which conditions such expansions can be applied to weakly nonlinear systems.

Strictly speaking, the concept of eigenmodes can be applied to any undamped, linear system of finite dimensions involving both kinetic and elastic energy, when the dynamics of the system are observed over a time scale which is large compared with the "characteristic time" of the system. The characteristic time corresponds to the time taken by a wave to propagate from an internal excitation point to the edges of the finite domain defined by the system. In Chap. 5 this notion will be extended to damped systems by introducing the concept of complex modes.

In the present chapter, the discussion is restricted to real modes. The basic mathematical properties of modes are presented, as well as general methods to calculate them. We illustrate these concepts using some examples linked to

string and percussion instruments. The acoustics of wind instrument resonators is considered in Chap. 7, where some results of the present chapter are used, drawing on the analogies outlined in Table 1.1 in Chap. 1.

3.2 Time Scale: Transition from Wave to Mode

When a continuous elastic medium (either solid or fluid), of finite size, is perturbed by an external stimulus, then the disturbance propagates away from the excitation point. The propagation speed of the disturbance depends on the inertial properties (density) and elasticity (compressibility, Young's moduli, and Poisson's ratios) of the medium. As long as the disturbance does not reach the boundaries of the medium, a *wave* approach such as the one outlined in Chap. 1 and developed in Chap. 4 is a suitable means of describing the phenomenon. Taking L as being a characteristic dimension of the medium, and c as the propagation speed, we can define a *characteristic time* $t_c = L/c$, where this wave approach remains valid (see Fig. 3.2). When the disturbance reaches the boundaries of the domain, part of the energy is generally transmitted to the external medium, the remaining part being reflected inside. Two situations can occur

1. The interference between incident and reflected waves at the boundaries is *constructive*. This happens at frequencies for which the incident and reflected waves are in phase. In this case, the total energy for these frequencies tends to increase with time. Only energy losses due to absorption or transmission at the boundaries, and during the propagation through the medium itself, limit this growth. In the absence of dissipation, the energy increases indefinitely in the medium.
2. The interference between incident and reflected waves at the boundaries is *destructive*. In this case, the phase relationship is such that no energy growth is possible over time in the medium. Because of absorption, the amplitudes of the corresponding frequencies gradually decrease.

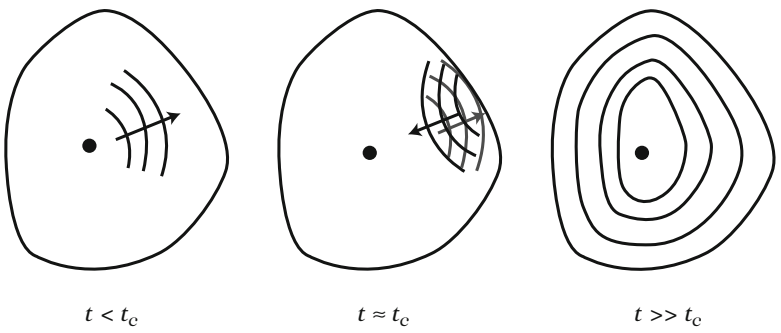

Fig. 3.2 Local vs. global approach of dynamic phenomena. t_c is the *characteristic time*

If the observation time is significantly larger than the characteristic time t_c of the medium, then the initial disturbance travels back and forth several times between the excitation point and the boundaries of the domain. In this scenario, it is therefore more useful to describe the phenomenon in a way that accounts for the fact that the energy of the system is distributed over a set of discrete frequencies. In the absence of dissipation, these frequencies are the "eigenfrequencies" of the finite medium. In the following paragraph, a rigorous definition will be introduced. As stated in the introduction, if a single eigenfrequency can be isolated (this can be achieved with a monochromatic excitation spectrum), then the spatial profile of the medium corresponds to an eigenshape.

It is always possible to describe the dynamics in terms of waves. We will show some applications of this approach in the next chapter. However, this wave approach quickly becomes very cumbersome and does not always provide a clear understanding of the physics. It is worth noting, finally, that, strictly speaking, the growth of an eigenmode needs a significant number of round-trips. Therefore, there is a definite intermediate period of time (between one and "a number of" t_c), where both the "wave" approach and the "mode" approach are acceptable.

3.3 Definitions and Basic Properties of the Eigenmodes

An eigenmode, for a discrete system or for a continuous medium with finite dimensions, is an eigensolution of a boundary value problem without a source (in the mathematical sense). In practice, this means that they are solutions of the equations describing the system without external excitation. If the system is conservative, these solutions are sinusoidal in time and are in phase (or in anti-phase): "standing waves" are obtained. The restriction to conservative media at this stage may be surprising as dissipation is essential for musical instruments, but before we consider musical instruments it is first important to understand the properties of the eigenmodes for this limiting reference case.

3.3.1 Discrete System

A discrete system has a finite number of degrees of freedom. In linear dynamics, the equations of motion of a discrete conservative system can be written in the general form:

$$\mathbb{M}\ddot{\boldsymbol{\xi}} + \mathbb{K}\boldsymbol{\xi} = 0, \tag{3.1}$$

where $\boldsymbol{\xi}$ is a vector containing the variables which describe the motion of the system, $\mathbb{M}$ is the mass matrix, and $\mathbb{K}$ the stiffness matrix. Each component of $\boldsymbol{\xi}$ is a function

of time. Matrices $\mathbb{M}$ and $\mathbb{K}$ are symmetrical. The general form of Eq. (3.1) is the same as that obtained for a discretized continuous medium, using finite element or finite difference methods (see Chap. 1).

In Chap. 2, it was shown how the eigenvectors and eigenfrequencies of an SDOF oscillator can be found. Let us now define the vector $\boldsymbol{w}$ and the matrix $\mathbb{M}_K$:

$$\boldsymbol{w} = \begin{pmatrix} \boldsymbol{\xi} \\ \dot{\boldsymbol{\xi}} \end{pmatrix} \; ; \; \mathbb{M}_K = \begin{pmatrix} \mathbf{0} & \mathbb{I} \\ -\mathbb{M}^{-1}\mathbb{K} & \mathbf{0} \end{pmatrix} , \tag{3.2}$$

so that Eq. (3.1) becomes: $\dot{\boldsymbol{w}} = \mathbb{M}_K \boldsymbol{w}$.

By definition, the eigenvectors of $\mathbb{M}_K$ must fulfill the condition: $\mathbb{M}_K \boldsymbol{w} = \lambda \boldsymbol{w}$, or

$$\dot{\boldsymbol{\xi}} = \lambda \boldsymbol{\xi} \; ; \quad -\mathbb{M}^{-1}\mathbb{K}\boldsymbol{\xi} = \lambda \dot{\boldsymbol{\xi}} \text{ , from which } \mathbb{K}\boldsymbol{\xi} = -\lambda^2 \mathbb{M}\boldsymbol{\xi} . \tag{3.3}$$

Denoting $\lambda^2 = -\omega^2$, the eigenfrequencies are the roots ω_n of the characteristic polynomial:

$$\det\left[-\omega^2 \mathbb{M} + \mathbb{K}\right] = 0 . \tag{3.4}$$

The number of roots is finite. These roots are real for a conservative system [16]. The eigenvectors (or *eigenshapes*) $\boldsymbol{\Phi}_n$ are therefore the nonzero solutions of the following equation:

$$\left[-\omega_n^2 \mathbb{M} + \mathbb{K}\right] \boldsymbol{\Phi}_n = 0 . \tag{3.5}$$

Important Property Since Eq. (3.5) is indeterminate, the components of $\boldsymbol{\Phi}_n$ are defined up to a multiplying factor.

The set $(\omega_n, \boldsymbol{\Phi}_n)$ defines the eigenmodes of the system. The mathematical theory of spectral analysis shows that the shapes $\boldsymbol{\Phi}_n$ form an $\mathbb{M}$- and $\mathbb{K}$-orthogonal basis of the vector space corresponding to the small motion of the system, which means

$${}^t\boldsymbol{\Phi}_m \mathbb{M} \boldsymbol{\Phi}_n = 0 \text{ and } {}^t\boldsymbol{\Phi}_m \mathbb{K} \boldsymbol{\Phi}_n = 0 \quad \text{for} \quad m \neq n , \tag{3.6}$$

where ${}^t\boldsymbol{V}$ represents the transpose of vector $\boldsymbol{V}$.

Demonstration

Let us write (3.5) for two specific eigenmodes n and m. We obtain

$$\omega_n^2 \mathbb{M} \boldsymbol{\Phi}_n = \mathbb{K} \boldsymbol{\Phi}_n \quad \text{and} \quad \omega_m^2 \mathbb{M} \boldsymbol{\Phi}_m = \mathbb{K} \boldsymbol{\Phi}_m . \tag{3.7}$$

(continued)

Multiplying both sides of the first expression by ${}^t\boldsymbol{\Phi}_m$ and, similarly, both sides of the second expression by ${}^t\boldsymbol{\Phi}_n$, we obtain

$$ {}^t\boldsymbol{\Phi}_m \omega_n^2 \mathbb{M} \boldsymbol{\Phi}_n = {}^t\boldsymbol{\Phi}_m \mathbb{K} \boldsymbol{\Phi}_n \quad \text{and} \quad {}^t\boldsymbol{\Phi}_n \omega_m^2 \mathbb{M} \boldsymbol{\Phi}_m = {}^t\boldsymbol{\Phi}_n \mathbb{K} \boldsymbol{\Phi}_m \, . \tag{3.8} $$

We now transpose the second expression, which leads to:

$$ \omega_m^2 {}^t\boldsymbol{\Phi}_m {}^t\mathbb{M} \boldsymbol{\Phi}_n = {}^t\boldsymbol{\Phi}_m {}^t\mathbb{K} \boldsymbol{\Phi}_n \, . \tag{3.9} $$

Given the symmetry properties of $\mathbb{M}$ and $\mathbb{K}$, the last equality becomes

$$ {}^t\boldsymbol{\Phi}_m \omega_m^2 \mathbb{M} \boldsymbol{\Phi}_n = {}^t\boldsymbol{\Phi}_m \mathbb{K} \boldsymbol{\Phi}_n \, . \tag{3.10} $$

By comparing the first expression of (3.8) with (3.10), we find

$$ \left(\omega_n^2 - \omega_m^2\right) {}^t\boldsymbol{\Phi}_m \mathbb{M} \boldsymbol{\Phi}_n = 0, \tag{3.11} $$

from which the expressions (3.6) are derived, since the eigenfrequencies are different.[2]

The orthogonality properties mean that the inertia and stiffness forces involved in a given eigenmode do not develop energy in the motion of the other modes. A mechanical independence exists between two distinct modes.

In theory, one can take advantage of this orthogonality to expand any solution of this problem onto the eigenmodes of the system. Thus, if the system is excited by a distribution of forces f, its motion is described as:

$$ \mathbb{M} \ddot{\boldsymbol{\xi}} + \mathbb{K} \boldsymbol{\xi} = \boldsymbol{f} \, . \tag{3.12} $$

The spectral theory shows that the eigenmodes form a *complete* system. As a consequence any solution of Eq. (3.12) yields a unique projection on the eigenmodes basis [15]. This projection can be written as:

$$ \boldsymbol{\xi} = \sum_n \boldsymbol{\Phi}_n q_n(t) \, . \tag{3.13} $$

The functions $q_n(t)$ are referred to as the *generalized displacements* or the *modal participation factors*. By substituting (3.13) into (3.12), and by making a inner product on both sides with any eigenvector $\boldsymbol{\Phi}_m$, we find, (after eliminating the zero products when $m \neq n$):

$$ \langle \boldsymbol{\Phi}_n, \mathbb{M} \boldsymbol{\Phi}_n \rangle \ddot{q}_n + \langle \boldsymbol{\Phi}_n, \mathbb{K} \boldsymbol{\Phi}_n \rangle q_n = \langle \boldsymbol{\Phi}_n, \boldsymbol{f} \rangle \, , \tag{3.14} $$

[2] It is shown, see, e.g., [18], that the orthogonality properties can be extended to the case of multiple eigenvalues.

where the notation $\langle\ ,\ \rangle$ represents the inner product: $\langle \boldsymbol{x}, \boldsymbol{x}' \rangle = {}^t\boldsymbol{x}\boldsymbol{x}'$. Equation (3.14) expresses the decoupling of generalized displacements. Each of these displacements is described by the differential equation of an independent SDOF oscillator. The quantity

$$m_n = \langle \boldsymbol{\Phi}_n, \mathbb{M}\boldsymbol{\Phi}_n \rangle \tag{3.15}$$

is the *modal mass* of the mode n. Like the eigenshapes, the modal masses are defined up to a constant multiplicative factor. Similarly, the quantities

$$\kappa_n = \langle \boldsymbol{\Phi}_n, \mathbb{K}\boldsymbol{\Phi}_n \rangle \tag{3.16}$$

are the modal stiffnesses. Note that:

$$\kappa_n = m_n {\omega_n}^2 . \tag{3.17}$$

Finally, the quantity

$$f_n = \langle \boldsymbol{\Phi}_n, \boldsymbol{f} \rangle \tag{3.18}$$

represents the projection of the external forces onto the mode n. In practice, if the inner product is zero, it is not possible to excite the corresponding mode. This occurs, for example, if a string is attached at a position corresponding to a node of a soundboard mode: in this case, the string cannot excite this mode.

In view of these definitions, we can rewrite the equation of each oscillator in the following generic form:

$$\ddot{q}_n + \omega_n^2 q_n = \frac{f_n}{m_n} . \tag{3.19}$$

The Fourier transform of $\boldsymbol{\xi}$ [Eq. (3.13)] becomes

$$\boldsymbol{\Xi}(\omega) = \sum_n \boldsymbol{\Phi}_n \frac{f_n}{m_n} \frac{1}{\omega_n^2 - \omega^2} . \tag{3.20}$$

The right-hand side of this expression is a sum of resonant terms. Consequently, if the system is forced at a frequency ω close to one particular eigenfrequency ω_n, the amplitude of that term will tend to infinity. In such a situation, the assumption of linearity for the system is no longer justified, and other tools for describing the nonlinear phenomena must be used (see Chap. 8).

Note 1: Since the eigenvectors are defined up to a constant multiplicative factor C, (3.15) shows that the modal mass is proportional to C^2. Consequently, (3.18) shows that f_n is proportional to C and (3.19) indicates that q_n is proportional to C^{-1}. In summary, (3.13) shows that the solution $\boldsymbol{\xi}$ is independent of C.

Note 2: The expression *normal mode* is sometimes used to designate an eigenmode *normalized* by an arbitrary constant. This constant can either be the modal mass of the mode n, or any other appropriate constant (the total energy of the system, the modal mass of the fundamental...), depending on the physical context.

3.3.1.1 Energy Approach

The total kinetic energy of the system is

$$\begin{aligned}\mathscr{E}_c = \frac{1}{2}\langle\dot{\boldsymbol{\xi}}, \mathbb{M}\dot{\boldsymbol{\xi}}\rangle &= \frac{1}{2}\langle\sum_n \boldsymbol{\Phi}_n\dot{q}_n(t), \mathbb{M}\sum_m \boldsymbol{\Phi}_m\dot{q}_m(t)\rangle \\ &= \frac{1}{2}\sum_n\sum_m\langle\boldsymbol{\Phi}_n, \mathbb{M}\boldsymbol{\Phi}_m\rangle\dot{q}_n(t)\dot{q}_m(t) \\ &= \frac{1}{2}\sum_n m_n\dot{q}_n^2(t).\end{aligned} \tag{3.21}$$

Similarly, the elastic potential energy is

$$\mathscr{E}_p = \frac{1}{2}\langle\boldsymbol{\xi}, \mathbb{K}\boldsymbol{\xi}\rangle = \frac{1}{2}\sum_n \kappa_n q_n^2(t)\ . \tag{3.22}$$

Therefore, the total energy of the system is the sum of the modal energies:

$$\mathscr{E} = \mathscr{E}_c + \mathscr{E}_p = \frac{1}{2}\sum_n m_n\dot{q}_n^2(t) + \kappa_n q_n^2(t) = \sum_n \mathscr{E}_n\ . \tag{3.23}$$

3.3.2 Extension to Continuous Systems

Extending the results obtained for discrete systems to continuous (conservative) systems, within the framework of linear approximation, shows that an *infinite* set of eigenmodes exists with orthogonality properties related to mass and stiffness operators. These eigenmodes form a complete basis for any linear motion of the system. In this case, the eigenvectors $\boldsymbol{\Phi}_n$ defined for discrete systems become continuous eigenfunctions of space $\Phi(\boldsymbol{x})$ and the inner products are expressed in the form of integrals over the entire structure.

The equation of motion for linear continuous systems can be written as:

$$\mathscr{L}(y) + \ddot{y} = s(\boldsymbol{x}, t)\ , \tag{3.24}$$

where $y(\boldsymbol{x}, t)$ is the displacement (or one of its derivatives), $\mathscr{L}(y)$ a linear operator, function of y and of its derivatives, and $s(\boldsymbol{x}, t)$ a source term. It is necessary to add boundary and initial conditions to define a well-posed problem.[3]

3.4 Application to Vibrating Strings

As the name suggests, the basic sound generation mechanism in any string instrument is the vibration of the strings attached to the neck and soundboard. The soundboard is set into motion by the strings, which act as vibratory sources, and the vibrations of the soundboard are transformed into an acoustic pressure (see Fig. 3.3).

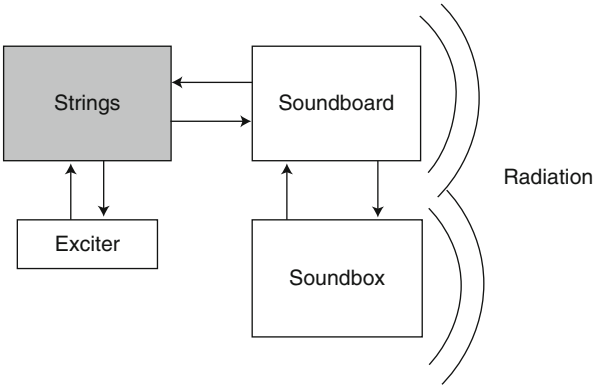

Fig. 3.3 Basic principles of string instruments. An exciter (finger, plectrum, hammer, and bow) sets one or more strings into vibration. This results in a string-exciter coupling which is either limited in time (plucked or struck strings) or permanent (bowed). The vibrations of the strings are transmitted to the soundboard via the bridge. The motion of the soundboard modifies the vibration of the strings slightly, especially if it is light and flexible, since it provides a moving end for the strings. The soundboard is usually coupled to an air cavity with sound holes (rose, f-holes). The radiation of the instrument is primarily due to the soundboard and soundholes and, to a lesser extent, to the back plate. The other parts of the instrument (neck, ribs) do not radiate much sound in general

[3] One can also define a vector $\boldsymbol{w} = \begin{pmatrix} y \\ \dot{y} \end{pmatrix}$ and separate time and space. Thus for the wave equation $\mathscr{L}(y) = -c^2 \frac{\partial^2 y}{\partial x^2}$, the equation to be solved can be written:

$$\dot{\boldsymbol{w}} = \boldsymbol{A}\boldsymbol{w} \text{ , where } \boldsymbol{A} = \begin{pmatrix} 0 & 1 \\ -c^2 \frac{\partial^2 y}{\partial x^2} & 0 \end{pmatrix} .$$

We therefore have a matrix operator $\boldsymbol{A}$, for which we can determine the eigenvectors and eigenvalues.

The same basic principles apply for all string instruments, though a wide variety of sounds and tone colors exist in this family. Variations in the excitation mechanisms and the material properties of the body are largely responsible for this diversity, although significant differences between the properties and regimes of vibration of the strings themselves are observable from one instrument to another. As an illustration, we will present some properties of bowed strings at the end of this section. These properties will be discussed in more detail in Chap. 11.

The experimental study of vibrating strings is a hard task, mainly because it is difficult to mechanically isolate them from their supporting frame: it is, for example, extremely hard in practice to obtain perfectly fixed boundary conditions. Moreover, the motion of a real string does not remain planar: there are always conditions of excitation, heterogeneities, and/or coupling conditions at the fixed ends that induce two polarizations and thus a resulting 3D motion. Finally, a coupling exists between the (dominant) transverse vibration and the longitudinal vibration (see Chap. 8).

In what follows, the fundamental behavior of string motion is reviewed, in the context of musical acoustics. The discussion is limited to the case of a planar transverse motion.

3.4.1 Heterogeneous String

For a one-dimensional string with density $\rho(x)$, tension $T(x)$, length L, and cross-section $S(x)$ (case of a heterogeneous string with variable diameter), the equation that describes the transverse displacement $y(x,t)$ is [see Eq. (1.11)]:

$$\rho(x)S(x)\frac{\partial^2 y}{\partial t^2} - \frac{\partial}{\partial x}\left[T(x)\frac{\partial y}{\partial x}\right] = f(x,t)\ , \tag{3.25}$$

where $f(x,t)$ is a linear density of force applied to the string, which can even be propagative, for example, in the case of a sliding finger. A variable tension $T(x)$ can be obtained if, for example, one hangs a string vertically, because of gravity. We deliberately choose this example of a heterogeneous string to highlight the general properties of the eigenmodes.

We limit ourselves in this section to cases where the boundary conditions are characterized either by a zero displacement or by a zero force. In Sect. 3.4.5 the extension to more complex situations will be examined, such as the cases (important in musical acoustics) of mass or elastic ends.

Let $\Phi_n(x)$ be the set comprising the eigenshapes of the string, for given boundary conditions. We expand a solution onto this basis by writing

$$y(x,t) = \sum_n \Phi_n(x) q_n(t)\ . \tag{3.26}$$

Multiplying both sides of (3.25) by any mode $\Phi_m(x)$, and integrating over the entire string, yields

$$\sum_n \ddot{q}_n(t) \int_0^L \Phi_n(x)\Phi_m(x)\rho(x)S(x)dx - \sum_n q_n(t) \int_0^L \Phi_m(x)\frac{d}{dx}\left(T(x)\frac{d\Phi_n(x)}{dx}\right)dx = \int_0^L \Phi_m(x)f(x,t)dx\,, \tag{3.27}$$

which can be rewritten in a symbolic form:

$$\mathscr{M}\,(\ddot{y}, \Phi_m) + \mathscr{K}\,(y, \Phi_m) = \langle f, \Phi_m \rangle\,. \tag{3.28}$$

Equation (3.28) is very general and can be applied to any continuous conservative system. The symbol $\mathscr{M}$ designates the mass operator, and $\mathscr{K}$ is the stiffness operator.

3.4.1.1 Orthogonality of the Eigenmodes

Consider a given eigenmode $\Phi_n(x)$. It must satisfy Eq. (3.25) for the case where the source term $f(x,t) = 0$:

$$-\omega_n^2\rho(x)S(x)\Phi_n(x) = \frac{d}{dx}\left[T(x)\frac{d\Phi_n(x)}{dx}\right]\,. \tag{3.29}$$

Using a similar method as used previously for discrete systems, we multiply both sides by $\Phi_m(x)$ and we integrate over the string's length. This gives

$$\omega_n^2 \int_0^L \Phi_n(x)\Phi_m(x)\rho(x)S(x)dx + \int_0^L \Phi_m(x)\frac{d}{dx}\left(T(x)\frac{d\Phi_n(x)}{dx}\right)dx = 0\,. \tag{3.30}$$

To simplify the working, the following notation is used:

$$\mathscr{P}_M(m,n) = \int_0^L \Phi_n(x)\Phi_m(x)\rho(x)S(x)dx \tag{3.31}$$

and

$$\mathscr{P}_T(m,n) = \int_0^L T(x)\frac{d\Phi_m(x)}{dx}\frac{d\Phi_n(x)}{dx}dx\,. \tag{3.32}$$

After integration by parts of the second term, the equality (3.30) becomes

$$\omega_n^2 \mathscr{P}_M(m,n) = \mathscr{P}_T(m,n) - \left[\Phi_m(x)T(x)\frac{d\Phi_n(x)}{dx}\right]_0^L . \tag{3.33}$$

Writing the same equation for both indices (n, m) yields

$$(\omega_m^2 - \omega_n^2)\mathscr{P}_M(m,n) = \left[\Phi_m(x)T(x)\frac{d\Phi_n(x)}{dx} - \Phi_n(x)T(x)\frac{d\Phi_m(x)}{dx}\right]_0^L , \tag{3.34}$$

and

$$(\omega_m^2 - \omega_n^2)\mathscr{P}_T(m,n) = \left[\omega_m^2\Phi_m(x)T(x)\frac{d\Phi_n(x)}{dx} - \omega_n^2\Phi_n(x)T(x)\frac{d\Phi_m(x)}{dx}\right]_0^L . \tag{3.35}$$

With the assumptions made on the boundary conditions (i.e., zero displacement or zero force), the terms between brackets are zero. Therefore, if $m \neq n$, the orthogonality of the eigenmodes with regard to mass and stiffness can be written as:

$$\mathscr{P}_M(m,n) = 0 \;\; ; \;\; \mathscr{P}_T(m,n) = 0 . \tag{3.36}$$

The kinetic and potential energies can be expressed as functions of these quantities:

$$E_c = \frac{1}{2}\sum_{n,m}\mathscr{P}_M(m,n)\,\dot{q}_n\dot{q}_m \;\; ; \;\; E_p = \frac{1}{2}\sum_{n,m}\mathscr{P}_T(m,n)\,q_n q_m . \tag{3.37}$$

Since the products $\mathscr{P}_M$ and $\mathscr{P}_T$ are zero for $m \neq n$, the energy is thus the sum of the energy of the modes (see Sect. 3.3.1.1).

Notes The orthogonality properties (3.36) are not related to any particular form of the solutions $\Phi(x)$ (sinusoidal or other). The demonstration here is valid for a heterogeneous string, for which the eigenfunctions are not explicitly known.

The previous results are also valid for a mode with a zero eigenfrequency. Equation (3.29) then shows that we must have $Td\Phi/dx =$ constant, which occurs when both boundary conditions are of "zero force" type. We then obtain $\Phi =$ constant as one of the solutions to the problem (this corresponds to a globally undeformed displacement, also known as a *rigid body mode*). To achieve such boundary conditions in the case of strings, we can think of rings sliding on rails orthogonal to the string, but it is a little bit exotic in the context of musical applications. However, an equation of the form (3.25) can be found in other contexts (longitudinal vibrations of bars and sound pipes) where the present remark then makes full sense.

3.4.1.2 Generalized Displacements

As a consequence of the orthogonality of the eigenmodes, and by taking Eq. (3.29) into account, (3.28) becomes

$$\ddot{q}_n(t) + \omega_n^2 q_n(t) = \frac{f_n(t)}{m_n}\,, \tag{3.38}$$

where the modal mass of the mode n is

$$m_n = \int_0^L \Phi_n^2(x)\rho(x)S(x)dx, \tag{3.39}$$

and where

$$f_n(t) = \int_0^L f(x,t)\Phi_n(x)dx \tag{3.40}$$

is the projection of the force density on the mode n. The modal stiffness is equal to:

$$\kappa_n = m_n\omega_n^2 = \int_0^L T\left(\frac{d\Phi_n}{dx}\right)^2 dx\,. \tag{3.41}$$

N.B. *In general, finding the modal mass m_n is easier than finding the modal stiffness κ_n. Since ω_n is known, the modal stiffness is most often determined using the first equality in Eq. (3.41).*

A set of oscillator equations is obtained for the generalized displacement of a continuous system, in the same way as for discrete systems. The main difference is that, for a continuous system, the number of independent differential equations is infinite in theory. In practice, however, a truncation of modes is made, depending on the frequency range under examination. In musical acoustics, we are primarily interested in the frequency domain corresponding to the audible range. This range might be further restricted in view of other considerations, such as damping or the spectral width of the excitation.

To solve the problem related to each generalized displacement, the methods and results presented in Chap. 2 devoted to the oscillator are of direct relevance. Damping phenomena will be introduced later in Chap. 5. The differential equations to be solved require a knowledge of the initial conditions. In the broad sense, these initial conditions include cases where the excitation is known starting from $t = -\infty$ (see Chap. 2).

Consider the case where the string is set into motion at a particular instant of time ($t = 0$) with initial profile $y(0,t)$ and initial velocity $\dot{y}(0,t)$. We can write as:

$$y(0,t) = \sum_n \Phi_n(x)q_n(0). \tag{3.42}$$

A similar expression can be written for the initial velocity. The mass and stiffness orthogonality of the modes yields the initial conditions for the displacements $q_n(t)$:

$$q_n(0) = \frac{1}{m_n} \int_0^L \rho(x) S(x) y(0,t) \Phi_n(x)\, dx$$

and (3.43)

$$\dot{q}_n(0) = \frac{1}{m_n} \int_0^L \rho(x) S(x) \dot{y}(0,t) \Phi_n(x)\, dx\,.$$

This leads to the result:

$$q_n(t) = \frac{1}{m_n \omega_n} \int_0^t f(\theta) \sin \omega_n (t-\theta)\, d\theta + q_n(0) \cos \omega_n t + \dot{q}_n(0) \frac{\sin \omega_n t}{\omega_n}\,. \tag{3.44}$$

Denoting $g_n(t) = \frac{\sin \omega_n t}{\omega_n}$, the first term of $q_n(t)$ is the convolution $f_n(t) \star g_n(t)$, where $g_n(t)$ is the Green's function of the oscillator corresponding to the nth-mode of the string (Note: see Chap. 2 and compare (3.44) with (2.20)).

3.4.1.3 Impulse Response of a String

In the particular case where $f_n(t)$ is a Dirac delta function of the form $f_{n0}\ \delta(t)$, its Laplace transform is a constant $F_n(s) = f_{n0}$. The expression (3.44) can then be reduced to:

$$q_n(t) = \frac{f_{n0}}{m_n} \frac{\sin \omega_n t}{\omega_n} + q_n(0) \cos \omega_n t + \dot{q}_n(0) \frac{\sin \omega_n t}{\omega_n}\,. \tag{3.45}$$

The *impulse response for the nth-mode of the string* is obtained. Some remarks can be made

1. An equivalence exists between the expressions of $q_n(t)$ obtained for the impulse excitation and the initial velocity condition, respectively. In other words, the string motion is identical, if the vibration is generated with an initial velocity profile or with a spatial distribution of forces whose time dependence is a Dirac delta function.
2. If the excitation also occurs at an infinitesimally small point in space, i.e., located at the point $x = x_0$, it is written $f(x,t) = A\delta(x - x_0)\delta(t)$. In this case, the result is $f_n(t) = \langle f(x,t), \Phi_n(x) \rangle = A\Phi_n(x_0)\delta(t)$. The magnitude of the the contribution of the nth mode to the string motion therefore depends on the value of the mode shape at the excitation point. In other words, the mode n of the string cannot be excited if the force is applied on one of its vibration nodes.

3. The Green's function for Eq. (3.25) can be defined as the function for which the applied force is[4]:

$$f(x,t) = T(x_0)\delta(t-t_0)\delta(x-x_0)\,.$$

The solution is:

$$g(x,t|x_0,t_0) = H(t-t_0)T(x_0)\sum_n \frac{\Phi_n(x)\Phi_n(x_0)}{m_n}\frac{\sin\omega_n(t-t_0)}{\omega_n}\,. \tag{3.46}$$

This solution illustrates the reciprocity between the source (at position x_0) and the receiver (at position x). For the constant mode $\Phi(x) = 1$ (when it exists), one must replace the last ratio with $(t-t_0)$. In this case, the growth over time is compensated in practice by the damping.

3.4.2 Ideal String Fixed at Both Ends

The simplest case to be considered is the so-called *ideal* string rigidly fixed at both ends. An *ideal* string is homogeneous with density ρ, constant cross-section S, and uniform tension T. It is assumed that vibrations occur without damping and restricted to a single plane. This situation is far from a real string, but it can be considered as a reference case. The transverse displacement $y(x,t)$ of the string is then described by the wave equation:

$$\frac{1}{c^2}\frac{\partial^2 y}{\partial t^2} = \frac{\partial^2 y}{\partial x^2}\,, \tag{3.47}$$

where $c = \sqrt{\frac{T}{\rho S}}$ is the propagation speed of the transverse waves. For a harmonic wave of the form $y(x,t) = e^{j(\omega t - kx)}$, Eq. (3.47) yields *the dispersion equation* $D(\omega,k)$ which expresses the relationship between angular frequency ω and wavenumber k. We obtain

$$D(\omega,k) = \omega^2 - c^2k^2 = 0\,, \tag{3.48}$$

showing that the ratio between angular frequency and wavenumber is constant and equal to c, a general property of *non-dispersive* medium. For a string of length L rigidly fixed at both ends, the eigenmodes must fulfill the conditions:

$$\frac{d^2\Phi_n}{dx^2} + \frac{\omega^2}{c^2}\Phi_n = 0 \quad \text{with} \quad \Phi_n(0) = \Phi_n(L) = 0\,. \tag{3.49}$$

[4]The factor $T(x_0)$ is written here in the applied force term to be consistent with other Green's functions which will appear in later chapters of this book.

As a consequence, the solutions for the eigenfunctions are

$$\Phi_n(x) = \sin k_n x \,, \tag{3.50}$$

where the wavenumber values correspond to the discrete set:

$$k_n = \frac{n\pi}{L}. \tag{3.51}$$

Using Eq. (3.48), the discrete set of angular frequencies is

$$\omega_n = \frac{n\pi c}{L}, \quad \text{i.e., for the eigenfrequencies:} \quad f_n = \frac{nc}{2L} \,. \tag{3.52}$$

According to Eq. (3.39), the modal mass is $m_n = \frac{\rho SL}{2} = \frac{M_s}{2}$, where M_s is the total mass of the string. In this particular case, all modal masses are equal. It is worth remembering that the value of the ratio $m_n/M_s = 1/2$ is purely arbitrary, since the modal masses are defined up to a multiplicative factor. On the contrary, the multiplicative constants are suppressed in Eq. (3.21) showing that the kinetic energy $\mathscr{E}_n = \frac{1}{2} m_n \dot{q}_n^2$ has a physical meaning.

3.4.3 Initial Conditions and Starting Transients

Traditionally, string instruments are divided into three main families: plucked strings (guitar, harpsichord, harp, etc.), struck strings (piano, hammered dulcimer, etc.), and bowed strings (violin, viola, cello, and double bass). This classification is based directly on the different excitation mechanisms of the string. In Chap. 1, a detailed physical description of the pluck was presented. In this chapter, the main focus is on vibration modes, and we will thus restrict ourselves in Sect. 3.4.4 with a simplified description of the pluck excitation.

In Sect. 3.4.7 there is some discussion on struck strings, with emphasis on the interaction between piano hammer and string. Finally, in Sect. 3.4.9, some properties of bowed strings are presented. The bow–string interaction is presented in detail in Chap. 11, focusing on the violin.

3.4.4 Plucked String

When plucked by a finger or a plectrum, the string is moved away from its initial equilibrium position. During the stick phase, a contact exists between the exciter and the string. When the restoring force due to tension (see Fig. 3.4) becomes slightly higher than the frictional force, the string slips under the finger (see Sect. 1.4.3.1 in Chap. 1).

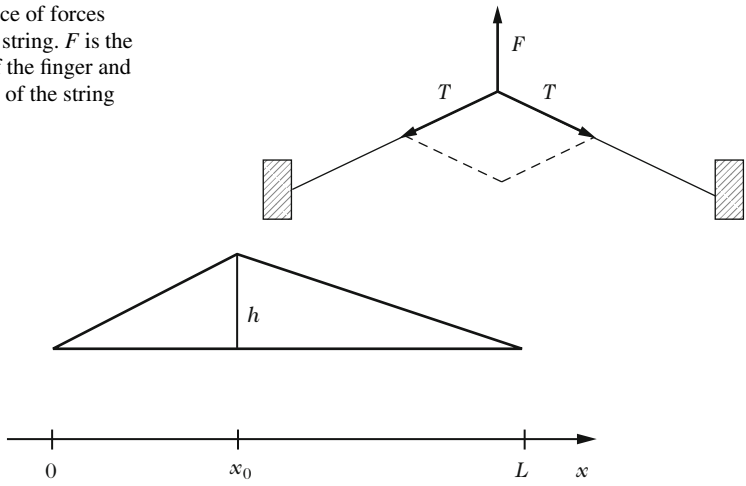

Fig. 3.4 Balance of forces for the plucked string. F is the pulling force of the finger and T is the tension of the string

Fig. 3.5 Simplified model of initial profile for a plucked string without stiffness

A simplified model for the starting transient of the string is presented below. It is assumed that the string leaves the exciter without initial velocity at string position x_0 with the initial profile (see Fig. 3.5):

$$y(0,t) = \begin{cases} \frac{hx}{x_0} & \text{for} \quad 0 \le x \le x_0, \\ \frac{h(L-x)}{L-x_0} & \text{for} \quad x_0 \le x \le L\,. \end{cases} \tag{3.53}$$

Note The string shape here is a perfect triangle, which is not realistic because of the intrinsic stiffness of the string. If stiffness terms are added to the string equation, then this initial string shape will have to be revisited.

The modal method involves searching for solutions of the form indicated in Eq. (3.26). This equation must be satisfied in particular at time $t = 0$, which leads to Eq. (3.43). Since the initial string velocity is taken equal to zero, we get $\dot{q}_n(0) = 0$, and the remaining unknown variables of the problem are the initial generalized displacements $q_n(0)$. Using the orthogonality properties of the modes, we find

$$q_n(0) = \frac{1}{m_n}\int_0^L \rho S y(0,t)\Phi_n(x)\,dx = \frac{1}{m_n}\int_0^L \rho S y(0,t)\sin k_n x\,dx\,, \tag{3.54}$$

from which we derive[5]

[5]In the particular case considered here, the constant term ρS can be moved out of the integrals in Eq. (3.54), and the orthogonality properties of the modes are reduced to:

$$q_n(0) = \frac{2hL^2}{n^2\pi^2 x_0(L-x_0)} \sin k_n x_0 \,. \tag{3.56}$$

The expression for $q_n(t)$ is provided by the equation of an oscillator with no applied force:

$$\ddot{q}_n + \omega_n^2 q_n = 0 \,, \tag{3.57}$$

which, given the initial displacement and velocity conditions, leads to $q_n(t) = q_n(0)\cos\omega_n t$. In summary, the general expression of the transverse displacement of the string is given by:

$$y(x,t) = \sum_n \frac{2hL^2}{n^2\pi^2 x_0(L-x_0)} \sin k_n x_0 \sin k_n x \cos\omega_n t \,. \tag{3.58}$$

Despite its simplicity, this last expression is very informative:

1. For an ideal plucked string rigidly fixed at both ends, the eigenfrequencies are integer multiples of a *fundamental* frequency $f_1 = c/2L$ which corresponds to the inverse of the period of vibration (Fig. 3.6). We obtain a *harmonic* spectrum.
2. The amplitudes of the modal components decrease as $1/n^2$ (see Fig. 3.7). As a consequence of this rapid decrease with regard to the rank n of the mode, one can consider representing the vibration with a limited number of components. In fact, the modal truncation depends on the problem under examination. In practice, a note played on the low E-string of the guitar (83 Hz fundamental) may contain 60–100 audible components, whereas notes produced on the high E-string (fundamental 330 Hz) only contain about 10–20 audible components.
3. The fact that the amplitude of mode n is proportional to $\sin k_n x_0$ shows that it is possible to suppress a given spectral component ω_n by exciting the string at points $(x_0)_p = \frac{pL}{n}$ where p is an integer $< n$.
4. The respective roles of the excitation position x_0 and observation position x are exchangeable in (3.58). This property is a consequence of the *principle of reciprocity*.
5. As x_0 tends to 0, $y(x,t)$ tends to

$$y(x,t) = \sum_n \frac{2h}{n\pi} \sin k_n x \cos\omega_n t \,. \tag{3.59}$$

$$\int_0^L \Phi_n(x)\Phi_m(x)\,dx = \begin{cases} 0 & \text{for } m \neq n, \\ \frac{L}{2} & \text{for } m = n \,. \end{cases} \tag{3.55}$$

This expression is a particular case. The formulation (3.54) is more general and this is the reason why we have kept it.

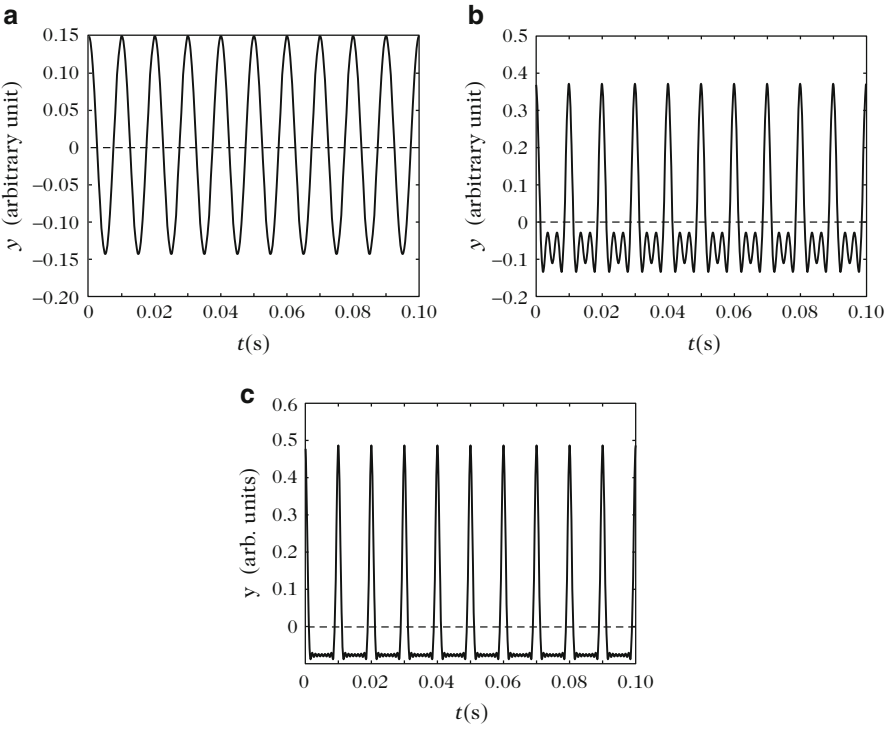

Fig. 3.6 Waveform of the displacement for an ideal string plucked at 7/8th of its length and observed at the same point. (**a**) One component; (**b**) three components; (**c**) ten components. As the number of components increases, the solution converges to a piecewise linear function, which corresponds to the exact solution (see Chap. 4)

The magnitudes of the components now vary as $1/n$, which means that if the excitation point is close to one end, then more harmonics are excited with significant amplitude. The corresponding sound will be "brighter".[6] By symmetry, the same argument can be made in the case where x_0 tends to L.

[6]The *brightness* of a sound is one of the perceptual attributes that characterize its timbre. A number of studies show that it is highly correlated to the *spectral centroid*, or *SC*, of the sound (indicating the "center of gravity of the spectrum"). If A_k is the amplitude of the frequency spectral component f_k of a sound containing N components, the SC is defined by $SC = \frac{\sum_{k=1}^{N} f_k A_k}{\sum_{k=1}^{N} A_k}$. This quantity characterizes the balance between bass and treble: a *dull* sound has a low *SC*, whereas a *bright* sound contains many high frequency components and therefore has a high *SC*.

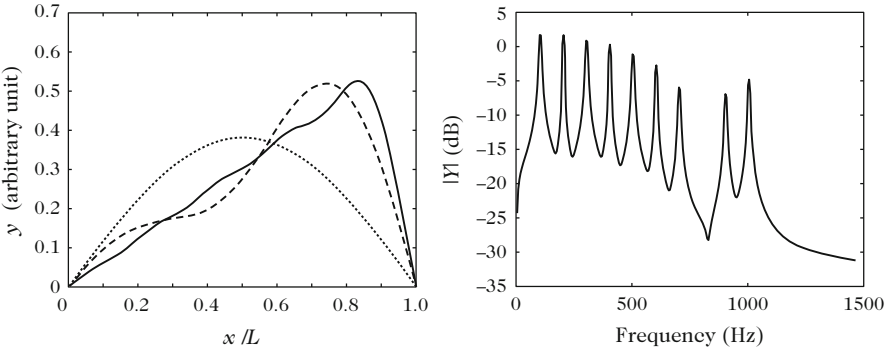

Fig. 3.7 *Left*: spatial shape of the string plucked at 7/8th of its length for a fixed time t. (*Dotted*) One mode; (*dashed*) three modes; (*solid line*) ten modes. *Right*: spectrum of the displacement of the string shown in Fig. 3.6 (ten components)

3.4.4.1 Force Transmitted by the String to the Bridge

As the string is moving, it exerts a time-dependent transverse force at both ends. To a first-order, we can assume that this force is proportional to the spatial derivative of the displacement, i.e., given the orientation of the x-axis (see Fig. 3.5):

$$F(0,t) = T\left(\frac{\partial y}{\partial x}\right)_{x=0} \quad \text{and} \quad F(L,t) = -T\left(\frac{\partial y}{\partial x}\right)_{x=L} . \tag{3.60}$$

In what follows, the bridge is arbitrarily taken as being located at $x = L$. The force transmitted by the string to the bridge can then be written as:

$$F(L,t) = -T\left(\frac{\partial y}{\partial x}\right)_{x=L} = -T\sum_n \frac{2hL}{n\pi x_0(L-x_0)} \cos k_n L \sin k_n x_0 \cos \omega_n t \, . \tag{3.61}$$

The amplitudes of the spectral components of the force vary as $1/n$, and tend towards a constant value when the excitation position x_0 gets closer to one of the ends. Thus, they decrease less rapidly with n than the displacement components do. Through sound synthesis, one can verify that the simulated sound of a "force" is "brighter" than the sound of the corresponding "displacement."

We will verify in Chap. 4 that, for an ideal string, the displacement waveform is piecewise linear (exact solution). The force waveform is therefore piecewise constant. Experimentally, it is observed that the force pulses are rounded, a consequence of string stiffness, limited bandwidth of the excitation, and damping. The truncation to ten modes shown here illustrates the resulting error on force and displacement waveforms (see Figs. 3.6 and 3.8).

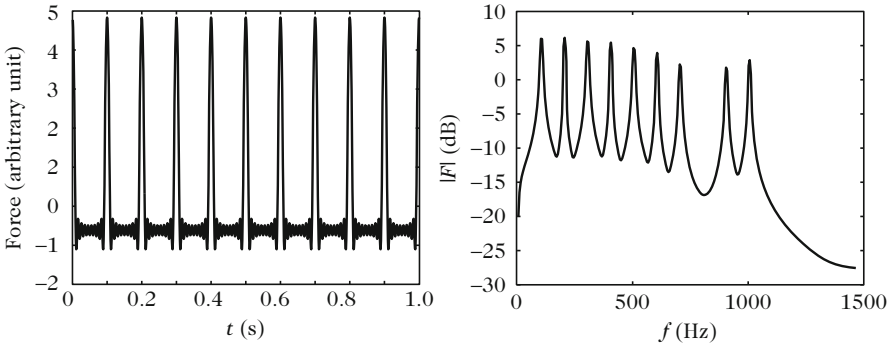

Fig. 3.8 Force transmitted by the string to the bridge. (*Left*) waveform (ten components); (*right*) corresponding spectrum. The force eigenfrequencies are identical to those of the displacement, but the comparison with Fig. 3.7 shows that the amplitudes of the force components with high order n (around 1000 Hz) are less attenuated compared to the components with lower order (around 100 Hz) than it is the case for the displacement component

3.4.5 String with a Moving End

In a string instrument, the strings do not radiate any significant acoustic energy, because their diameter is small compared to the acoustic wavelength (see Chap. 12). As an empirical proof, it is easy to carry out a simple experiment: stretch a string between your fingers and pluck it. You will only hear a sound when the string is brought close to your ear.

To radiate acoustic energy efficiently, the string needs to be coupled to a resonator with a large surface. This is the main role of the soundboard. As a consequence, the assumption of zero displacement at both ends of the string is unrealistic. It would imply that the soundboard is rigidly fixed and does not produce any sound.

We shall therefore now consider that at least one of the string's ends is moving. This boundary condition corresponds to the coupling of two continuous systems (string and soundboard), each of them presenting an infinite number of modes. A comprehensive model of such coupled systems will be presented in Chap. 6. Here, the effect of one particular mode (a single oscillator) of the soundboard on the string will be examined.

It is well-known (see Chap. 2) that such an oscillator behaves either like a spring or like a mass, depending on the ratio between the excitation frequency and the eigenfrequency of the oscillator. These two limiting cases will be studied, leaving the particular case where the oscillator behaves as a pure damper temporarily aside. This latter case will be studied in detail in Chap. 5. In actual fact, the soundboard itself is subjected to dissipation, because of internal losses and radiation, which we will also ignore for the moment.

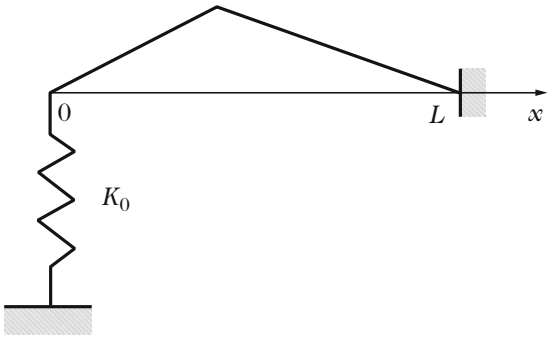

Fig. 3.9 String fixed at one of its ends (at position $x = 0$) to a spring of stiffness K_0

3.4.5.1 Purely Elastic End

Consider first the situation of a homogeneous string fixed to a spring of stiffness K_0 at point $x = 0$ (see Fig. 3.9). The balance of forces yields the boundary condition:

$$T\left(\frac{\partial y}{\partial x}\right)_{x=0} = K_0\, y(0,t)\ . \tag{3.62}$$

It is assumed that the displacement of the string remains equal to zero at the other end, i.e., $y(L,t) = 0$. To calculate the eigenmodes, we search for solutions of the form $y(x,t) = \Phi(x)\cos\omega t$. According to Eq. (3.47), the functions $\Phi(x)$ must satisfy the equation:

$$\frac{d^2\Phi}{dx^2} + k^2\Phi = 0 \tag{3.63}$$

and the two boundary conditions. Equation (3.63) with the condition $\Phi(L) = 0$ gives

$$\Phi_n(x) = \sin k_n(x - L). \tag{3.64}$$

The condition at $x = 0$ yields

$$\tan k_n L = -\frac{k_n T}{K_0}\ . \tag{3.65}$$

The index n in Eq. (3.65) shows that the condition is fulfilled for a discrete set of values of the variable k only. Equation (3.63) is, in turn, only satisfied for a discrete set[7] of functions $\Phi_n(x)$. Using Eq. (3.65), we can write:

[7]The solution $k_n = 0$ is excluded here, since it leads through (3.63) to the degenerate solution $\Phi_n(x) = 0\ \ \forall x$, because of the condition of zero displacement in $x = L$.

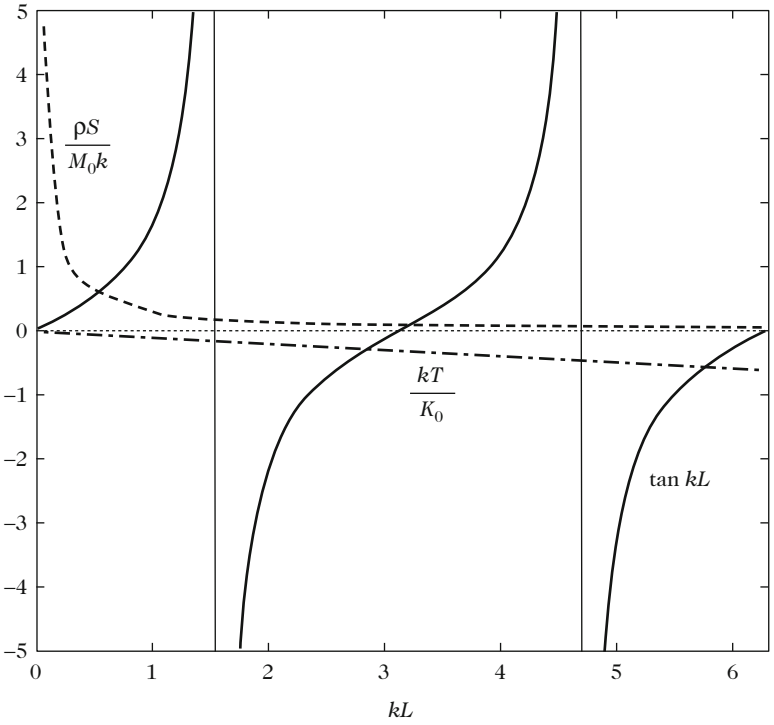

Fig. 3.10 Graphical representation of Eq. (3.65) for the case of a moving end. *Dotted line*: elastic end. *Dashed line*: string with a mass at one end

$$\Phi_n(x) = \sin k_n x + \frac{k_n T}{K_0} \cos k_n x \,. \tag{3.66}$$

The graphical representation of (3.65) (see Fig. 3.10) shows that the roots k_n are no longer multiples of k_1, as it was the case for the ideal string with fixed ends. As a consequence, the motion of the string is not periodic. The roots depart more and more from the ideal harmonic series as the rank n of the partial increases. The presence of a spring at one end of the string systematically leads to a *decrease* in the eigenfrequencies in comparison with the ideal case. This is not surprising as it corresponds to introducing a finite stiffness into the system, compared with the perfectly rigid case (equivalent to an infinite stiffness). Introducing flexibility in a system leads to a lowering of its eigenfrequencies.[8]

[8]One can also consider the introduction of a spring as an apparent increase in the length of the string, but with the condition that the length correction depends on the rank n of the partial. If one writes $k_n \Delta\ell = \arctan[k_n T/K_0]$, the roots are solutions of the equation $\tan k_n(L + \Delta\ell) = 0$. For the first modes, we have $\Delta\ell \simeq T/K_0$. This approach is very convenient for wind instruments.

Once the modes are determined, the initial values $q_n(0)$ of the generalized displacements can be derived from the integral expressed in Eq. (3.54). Equations (3.34) and (3.35) show that, for an isolated string, the modes are orthogonal with respect to mass, but are no longer orthogonal with respect to stiffness. However, one can generalize the concept of orthogonality to the whole system (string + spring) by considering the total potential energy.[9]

According to Eqs. (1.124), (3.62), and (3.37):

$$E_p = \frac{1}{2}\int_0^L T\left(\frac{\partial y}{\partial x}\right)^2 dx + \frac{1}{2}K_0 y^2(0,t)$$
$$= \frac{1}{2}\sum_{n,m}\left[\mathscr{P}_T(m,n) + K_0\Phi_n(0)\,\Phi_m(0)\right] q_n q_m \,.$$

However, according to Eq. (3.35), $\mathscr{P}_T(m,n) = -K_0\Phi_n(0)\,\Phi_m(0)$ for $n \neq m$. So, finally we get[10]

$$\mathscr{E}_p = \frac{1}{2}\sum_n \left[\kappa_n + K_0\Phi_n^2(0)\right] q_n^2 \quad \text{where} \quad \kappa_n = \mathscr{P}_T(n,n)\,. \tag{3.67}$$

3.4.5.2 String with a Mass at One End

The case of a homogeneous string with a mass at one end is now examined. It is assumed that the mass M_0 is located at position $x = 0$. The following boundary condition must then be satisfied[11]:

$$T\left(\frac{\partial y}{\partial x}\right)_{x=0} = M_0\,\frac{\partial^2 y}{\partial t^2}(0,t)\,. \tag{3.68}$$

[9] In (1.124), the term within the brackets corresponds to the input power at both ends. We get:

$$T\frac{\partial y}{\partial x}\frac{\partial y}{\partial t} = K_0 y\frac{\partial y}{\partial t} = \frac{\partial e_0}{\partial t} \quad \text{where} \quad e_0 = \frac{1}{2}K_0 y^2 \text{ in } x = 0.$$

[10] A similar problem will be tackled in Chap. 4 for a pipe loaded by a radiation impedance at low frequencies. We will see that, assuming $k_n\Delta\ell << 1$, where $\Delta\ell = T/K_0$, the moving end can be replaced by a fixed termination for the pipe with an end correction $\Delta\ell$ at the end $x = 0$. The calculations of the modes are simplified, and we can recover the term $K_0\Phi_n^2(0)$, considering the energy located between $x = -\Delta\ell$ and $x = 0$. This means that, instead of considering a boundary condition corresponding to a lumped element at $x = 0$, we consider a longer medium, with some particular parameters ρ, S, and T in the extension, and with a simple boundary condition, $y(-\Delta\ell, t) = 0$.

[11] We obtain identical results with the mass located at position $x = L$. In this latter case, there is a change of sign in the boundary condition.

It is assumed that the other end is fixed, i.e., $y(L,t) = 0$. The condition (3.68) involves time derivatives, which makes the resolution by Fourier transform difficult (see below). The method used here is the separation of variables. It involves testing the existence of standing waves of the form $y(x,t) = \Phi(x)w(t)$ and searching for those conditions under which the equations of the problem are verified. Inserting $y(x,t)$ in Eq. (3.47), we obtain:

$$\frac{\Phi}{c^2}\frac{d^2w}{dt^2} = w\frac{d^2\Phi}{dx^2} \,. \tag{3.69}$$

By grouping the terms involving the same variables, we derive

$$\frac{1}{c^2 w}\frac{d^2w}{dt^2} = \frac{1}{\Phi}\frac{d^2\Phi}{dx^2} = -\alpha^2, \tag{3.70}$$

where $-\alpha^2$ is a constant. The only way to satisfy the first equality of Eq. (3.70) is for both sides of the equality to be set as constant, since they involve a different variable (resp. t and x). Due to the boundary conditions, it will be now shown that the constant α is real.

The resolution of both differential equations in (3.70) yields the general solutions:

$$w(t) = A\cos c\alpha t + B\sin c\alpha t \quad \text{and} \quad \Phi(x) = C\cos\alpha x + D\sin\alpha x \,. \tag{3.71}$$

The boundary conditions for $x = 0$ and $x = L$ imply that:

$$\begin{aligned} &\Phi(L) = C\cos\alpha L + D\sin\alpha L = 0 \\ &\text{and} \quad T\frac{d\Phi}{dx}(0) = -\alpha^2 c^2 M_0 \Phi(0) \,. \end{aligned} \tag{3.72}$$

Thus α must fulfill the condition:

$$\tan\alpha L = \frac{\rho S}{\alpha M_0} \,, \tag{3.73}$$

and is therefore real.

Figure 3.10 shows that this equality can be obtained for a discrete set of wavenumbers only:

$$k_1 < k_2 < \ldots < k_n. \tag{3.74}$$

This leads to the eigenvalue equation:

$$\tan k_n L = \frac{\rho S}{M_0 k_n} \,. \tag{3.75}$$

The mass loading leads to an *increase* in the eigenfrequencies of the string and in turn to an *apparent decrease* in its length (see Fig. 3.10). The ideal case is obtained as M_0 tends to infinity in Eq. (3.75).

In the case of a mass-loaded end, the modes of the string are orthogonal with regard to stiffness, but not with regard to mass. For the string+mass system, the orthogonality can be extended by considering the total kinetic energy:

$$\mathscr{E}_c = \frac{1}{2}\sum_n \left[m_n + M_0\Phi_n^2(0)\right]\dot{q}_n^2 \quad \text{where} \quad m_n = \mathscr{P}_M(n,n). \tag{3.76}$$

Note The first consequence of the coupling between string and soundboard is to modify its eigenfrequencies. This is one cause of *inharmonicity* in the sound produced by the instrument. The coupling affects the lowest eigenfrequencies primarily, i.e., those for which the amplitude of the soundboard motion is the strongest, and thus where the assumption of perfect rigidity is the least satisfied.

Orthogonality Properties of a Heterogeneous String

Turning back to the general case of a heterogeneous string of length L (Eq. (3.25) without an applied force term), the goal is now to find the orthogonality properties of the eigenmodes when one end is fixed while the other end is connected to a mass M_L. With boundary conditions of the problem:

$$y(0,t) = 0 \quad \text{and} \quad -T(x)\frac{\partial y}{\partial x} = M_L\frac{\partial^2 y}{\partial t^2}, \ \text{at } x = L\,, \tag{3.77}$$

we obtain

$$\mathscr{P}_M(m,n) = \frac{t_n}{\omega_n^2}\delta_{mn} - M_L\Phi_m(L)\Phi_n(L), \tag{3.78}$$

where

$$t_n = \mathscr{P}_M(n,n) = \int_0^L T(x)\left[\frac{d\Phi_n(x)}{dx}\right]^2 dx\,. \tag{3.79}$$

This shows that the modes are orthogonal with regard to stiffness, but not with regard to mass. In conclusion, Eq. (3.38) becomes

$$\begin{aligned}\ddot{q}_n(t) + \omega_n^2 q_n(t) &= \frac{1}{t_n}\int_0^L \frac{\partial}{\partial x}\left(\frac{f(x,t)}{\rho(x)S(x)}\right)T(x)\frac{d\Phi_n(x)}{dx}dx \\ &= \frac{1}{t_n}\left[\frac{f(L,t)}{\rho(L)S(L)}M_L\Phi_n(L) + \omega_n^2\int_0^L f(x,t)\Phi_n(x)dx\right]\,.\end{aligned} \tag{3.80}$$

Fourier Domain Approach
Eigenmode decomposition can also be applied in the Fourier (or in the Laplace) domain. To illustrate this, the case of a homogeneous string with a mass at one end is presented. In the Fourier domain, the condition at the mass-loaded end (3.68) is

$$T\frac{d\mathscr{Y}}{dx} = M\omega^2\mathscr{Y}\ . \tag{3.81}$$

The Fourier transform of the wave equation (3.25) is the Helmholtz equation:

$$\frac{d^2\mathscr{Y}(\omega)}{dx^2} + \frac{\omega^2}{c^2}\mathscr{Y}(\omega) = -\frac{1}{T}F(x,\omega). \tag{3.82}$$

Let us now examine the case of a localized excitation, e.g., a Green's function $F(x,\omega) = T(x_0)\delta(x-x_0)$. The solution is expanded onto the *eigenfunctions* ψ_p of the equation:

$$\frac{d^2\psi_p}{dx^2} + \frac{\omega_p^2}{c^2}\psi_p = 0\ , \tag{3.83}$$

with the boundary conditions: $\psi(0) = 0$, and (3.81). In Eqs. (3.81) and (3.82), *ω is a parameter. Thus the eigenfunctions and their corresponding eigenfrequencies ω_p depend on frequency:* As a consequence, we do not get modes in the strict sense. Finally, we write: $\psi_p = \sin(\omega_p x/c)$, where

$$\tan\frac{\omega_p(\omega)L}{c} = \frac{T}{Mc}\frac{\omega_p(\omega)}{\omega^2}. \tag{3.84}$$

For a given ω, there is an infinite set of values for ω_p. The solution can then be expressed as a sum of functions $\psi_p(x)$:

$$\mathscr{Y}(\omega) = \sum_p \psi_p(x)Q_p(\omega). \tag{3.85}$$

These functions are orthogonal with regard to the mass, i.e., for a homogeneous string:

$$\int_0^L \psi_p(x)\psi_q(x)dx = \Lambda_p\delta_{pq}, \tag{3.86}$$

(continued)

where Λ_p is a constant and δ_{pq} the Kronecker symbol. All these functions satisfy Eq. (3.81) with a fixed ω. One can therefore write

$$\mathscr{Y}(\omega) = c^2 \sum_p \frac{\psi_p(x)\psi_p(x_0)}{\Lambda_p \left[\omega_p^2(\omega) - \omega^2\right]} . \tag{3.87}$$

If (3.84) is solved for a given frequency, (3.87) enables the calculation of the Fourier transform of $y(t)$, that is $\mathscr{Y}(\omega)$ and, by inverse Fourier transform, $y(t)$ itself. This approach is often used in acoustics, especially in room acoustics [27]. It is also systematically used in sound synthesis based on physical models by Rabenstein and Trautmann [37].

Note 1: The previously described orthogonality is *simple* for this conservative problem. In general, depending on the end impedances, one must build an adjoint problem, with an adjoint modes basis denoted $\overline{\psi_p}$. The *bi-orthogonality* between both families of modes is written:

$$\int_0^L \psi_p(x)\overline{\psi_q}(x)dx = \Lambda_p \delta_{pq} . \tag{3.88}$$

It turns out that the adjoint family is the family of the conjugates, which implies $\int_0^L \psi_p(x)\psi_q(x)dx = \Lambda_p \delta_{pq}$, even if the functions $\psi_p(x)$ are complex.

Note 2: Inverse transformation to the time domain, and therefore to the modes, is possible in the case studied above, but it is subtle. In the series (3.87), for a given frequency ω, only two functions $\psi_p(x)$ are resonant, which means that some terms of the series may have a zero denominator. Denoting their indices by n and $-n$, we have: $\omega_n = \pm\omega$ and both correspond to the same shape $\psi_n(x)$. By inserting $\omega_n = \pm\omega$ in (3.84), it can be seen that the two values of ω_n satisfy Eq. (3.75). As a consequence, both resonant terms of the series (3.87) have an infinite number of poles. Finally, one can check that $\psi_n(x) = \Phi_n(x)$. The residues theorem is used to return to the time domain (see the appendix at the end of this chapter). First, the Taylor expansion of the denominator $D(\omega) = \Lambda_n(\omega_n^2 - \omega^2)$ is written in the form $D(\omega) = D(\omega_n) + (\omega - \omega_n)D'(\omega_n)$, with:

$$\begin{aligned} D'(\omega_n) = \left[\frac{dD(\omega)}{d\omega}\right]_{\omega=\omega_n} &= \Lambda_n \left[2\omega_n \frac{d\omega_n}{d\omega} - 2\omega\right]_{\omega=\omega_n} \\ &= 2\Lambda_n\omega_n \left[\left(\frac{d\omega_n}{d\omega}\right)_{\omega=\omega_n} - 1\right]. \end{aligned} \tag{3.89}$$

(continued)

To calculate $d\omega_n/d\omega$ in ω_n, one needs to derive Eq. (3.84) with respect to ω. It is also necessary to explicitly calculate Λ_n. After some tedious calculations, we get

$$\Lambda_n \left[\left(\frac{d\omega_n}{d\omega} \right)_{\omega=\omega_n} - 1 \right] = -\frac{L_n}{2} \quad \text{with}$$
$$L_n = L + \frac{\Delta\ell}{1 + \left(\frac{\omega_n \Delta\ell}{c} \right)^2} \quad \text{where} \quad \Delta\ell = \frac{M}{\rho S} . \tag{3.90}$$

In addition, we find $t_n = TL_n\omega_n^2/(2c^2)$. By adding both terms with poles of Eq. (3.87), we finally obtain $\mathscr{Y}(\omega) = \sum \psi_n(x)Q_n(\omega)$, with:

$$-\omega^2 Q_n + \omega_n^2 Q_n = 2c^2 \psi_n(x_0)/L_n = T\psi_n(x_0)\omega_n^2/t_n. \tag{3.91}$$

This is in agreement with the expression (3.80), when $f(x,t) = T\delta(x - x_0)\delta(t)$.

3.4.6 *Influence of Spatial Width and Duration of the Excitation*

In practice, the excitation of a string is distributed over a segment of finite length. One can think, for example, of the width of a violin bow, of a piano hammer, or of a player's finger. Many string instruments (piano, guitar, harp, violin played pizzicato, etc...) are also excited over a finite time interval, corresponding to the duration of the interaction with the exciter. In this section, the effect of both the spatial width and finite duration of the excitation on the string's response are examined.

Note For simplicity, only the example of the ideal string fixed at both ends is treated here. In this case, we know that the eigenmodes are $\Phi_n(x) = \sin k_n x$. Nevertheless, the method developed here remains valid in the general case.

We first consider the situation presented in Fig. 3.11 where the string is excited by a force term comprising a Dirac delta function in time, and distributed over a string segment of width $2a$ centered at position x_0. We write[12]

$$f(x,t) = B\delta(t)g(x) \quad \text{with} \quad g(x) = \begin{cases} 1 & \text{if } x_0 - a \le x \le x_0 + a, \\ 0 & \text{elsewhere .} \end{cases} \tag{3.92}$$

[12]The coefficient B in this expression has the dimension of a mass divided by time ($[M][T]^{-1}$) because of the presence of the Dirac delta function.

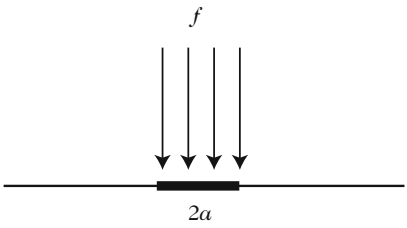

Fig. 3.11 Spatial width of the excitation of a string. The force f exerted on a string by a finger, a plectrum, a hammer, or a bow, is distributed over a finite width, here denoted $2a$

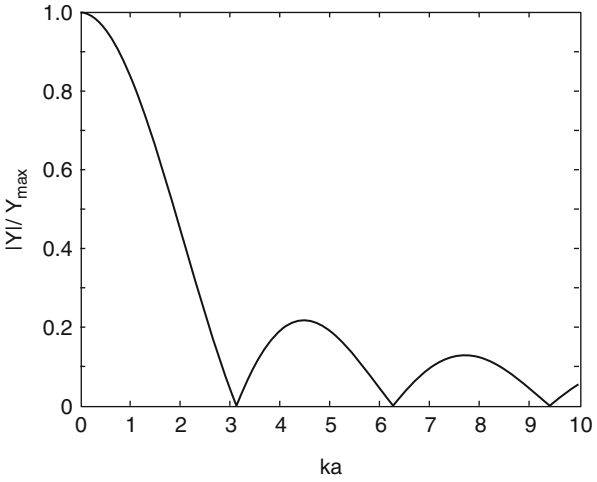

Fig. 3.12 Low pass filtering of the string displacement due to the width $2a$ of the exciter

We derive the projection of the applied force term on the mode n:

$$f_n = \langle f, \Phi_n \rangle = B\delta(t) \int_{x_0-a}^{x_0+a} \sin k_n x \, dx = 2aB\delta(t) \sin k_n x_0 \frac{\sin k_n a}{k_n a} \,. \tag{3.93}$$

Hence, for a string initially at rest, the displacement is

$$y(x,t) = 2aB \sum_n \frac{\sin k_n x \sin k_n x_0}{m_n} \frac{\sin k_n a}{k_n a} \frac{\sin \omega_n t}{\omega_n} \,. \tag{3.94}$$

The expression (3.94) shows that, compared to the case of a point excitation, the spatial width induces a *low pass filtering* of the string response, through the term in $\frac{\sin k_n a}{k_n a}$ (see Fig. 3.12). The first cutoff frequency f_c of this filter occurs when $ka = \pi$, i.e., $f_c = \frac{c}{2a}$.

Numerical Example For a piano wire of length $L = 62\,\text{cm}$, corresponding to the note C4 (fundamental $f_1 = 262\,\text{Hz}$), the propagation speed of the transverse

Fig. 3.13 Pulse of finite duration

waves is $c = 2Lf_1 = 325$ m/s. Taking $2a = 2$ cm as an order of magnitude estimate for the spatial window of excitation by the hammer, we find $f_c = 16$ kHz, which approximately corresponds to the upper limit of the audible spectrum.

- Now the effect of the finite duration of the interaction between string and exciter is investigated. We assume a spatially localized force density of the form:

$$f(x,t) = C\delta(x - x_0)h(t) \tag{3.95}$$

with

$$h(t) = \begin{cases} 1 & \text{for } 0 \le t \le 2\tau, \\ 0 & \text{for } t > 2\tau, \end{cases}$$

where C has a dimensions $[M][L][T]^{-2}$, and where 2τ represents the duration of the interaction between string and exciter (see Fig. 3.13).

From Eq. (3.44), and under the assumption of a string initially at rest, the generalized displacement of mode n is

$$q_n(t) = \frac{C\Phi_n(x_0)}{m_n\omega_n} \int_0^{2\tau} \sin\omega_n(t-\theta)d\theta, \tag{3.96}$$

which gives the string displacement:

$$\begin{cases} \text{For} \quad 0 \le t \le 2\tau \quad y(x,t) = 2\tau C \sum\limits_n \dfrac{\sin k_n x \sin k_n x_0}{m_n} \dfrac{1-\cos\omega_n t}{\omega_n^2 \tau}, \\ \text{For} \quad t > 2\tau \quad y(x,t) = 2\tau C \sum\limits_n \dfrac{\sin k_n x \sin k_n x_0}{m_n} \dfrac{\sin\omega_n \tau}{\omega_n \tau} \dfrac{\sin\omega_n(t-\tau)}{\omega_n} \end{cases}. \tag{3.97}$$

As for the spatial width analysis, the finite duration of the interaction force results in a low pass filtering of the response $y(x,t)$ through the term $\frac{\sin \omega_n \tau}{\omega_n \tau}$. Returning back to the example of the piano wire, we notice that the calculation of the cutoff frequency, defined by the first zero of the previous function, yields here $f_c = \frac{1}{2\tau}$. By taking $2\tau = 1$ ms as an order of magnitude typically observed on piano wires, (see, for example, [3]), we find $f_c = 1$ kHz. This cutoff frequency is significantly lower than the one resulting from the spatial width of the excitation.

3.4.7 Struck String

The previous considerations give some understanding of the effects of finite width and duration on the string spectrum. Returning now to a more accurate description of the piano string, we must take the mass M_h of the hammer and its initial impact velocity V_0 into account. This description will be refined later with the introduction of damping mechanisms both in the string and in the hammer's felt, as shown in Chap. 5.

During the contact phase between hammer and string, some of the initial kinetic energy is transformed into elastic compression energy of the felt (see Fig. 3.14).

The resulting compression force is imparted to the string and gives rise to transverse traveling waves. These waves are initiated on both sides of the impact position. As a result of the magnitude of the propagation speed of the bending wave on the string, and the small distance between the impact position and one of its ends (the agraffe side), the waves propagating on this "shorter side" of the string reach the hammer before it leaves the string (see Figs. 3.14 and 3.15). As a consequence, the action of the wave modifies the compression force, resulting in a modulation of the interaction force between hammer and string. These modulations can be intense enough to cause the hammer to bounce back and, in turn, a discontinuity of the force in the lower range of the instrument can be observed (see Fig. 3.16).

An abundance of literature on the analytical and numerical modeling of the hammer–string interaction is available; see, for example, [7, 11, 22]. We will see a similar 2-D example in Chap. 14: the mallet-membrane interaction in timpani.

3.4.8 Driving-Point and Transfer Admittance

The motion of the end of the string that is fixed to the bridge induces vibrations in the soundboard. The modal approach is an appropriate tool to characterize this transfer, both theoretically and experimentally. In order to study this coupling, which is essential for the understanding of string instruments, we start by defining the concept of mechanical *admittance* (or mobility) (see also Sect. 1.6 in Chap. 1), before studying its frequency behavior in detail.

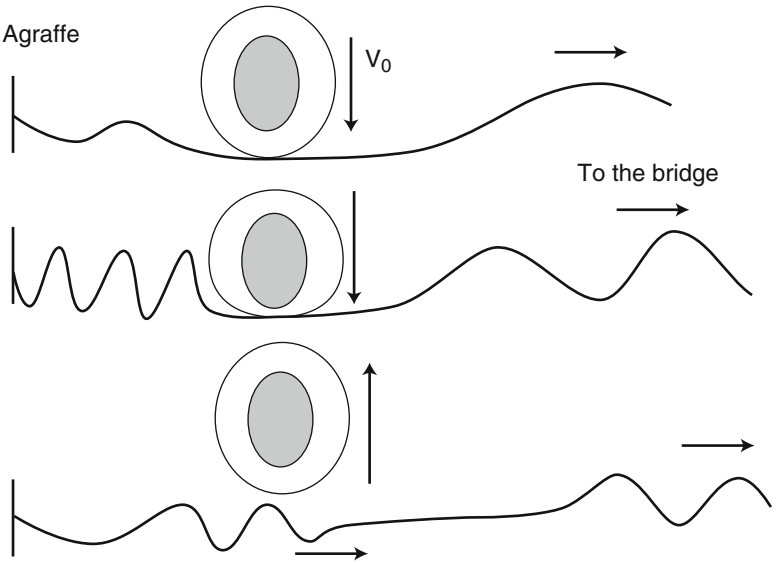

Fig. 3.14 Hammer–string interaction. (*1*) The hammer with initial impact velocity V_0 comes into contact with the string. The felt is compressed and a force is imparted to the string. Transverse waves are developed on the string on both sides of the hammer. (*2*) As long as string and hammer stay in contact, the waves developed on the shorter side of the string stay confined between the agraffe and the hammer, which prevents propagation towards the bridge. (*3*) After a few milliseconds, the reaction of the string pushes the hammer back and these waves are free to propagate

Consider a continuous structure, a piano soundboard, for example, subjected to forces and moments. In general, for numerical and/or experimental reasons, it is necessary to work on a discretized version of this structure, i.e., on a mesh containing a finite number N of areas whose dimensions are small in comparison with the wavelength. These small areas are commonly referred to as"points." This amounts to considering the structure as a discrete system with N degrees of freedom (see Fig. 3.17).

At each point of the mesh, the motion is characterized by three translation components and three rotation components. In what follows, the velocity is treated as a variable. Similarly, the external actions at each point reduce to three force components and three moment components [9].

Admittances are defined in the frequency domain. At each point, the velocity components of the motion (V_k) are linked through a 6×6 matrix to the force and moment components, denoted F_l. The *admittance matrix at one point* $\mathbb{Y}$ is defined as:

$$\boldsymbol{V} = \mathbb{Y}\boldsymbol{F}\,. \tag{3.98}$$

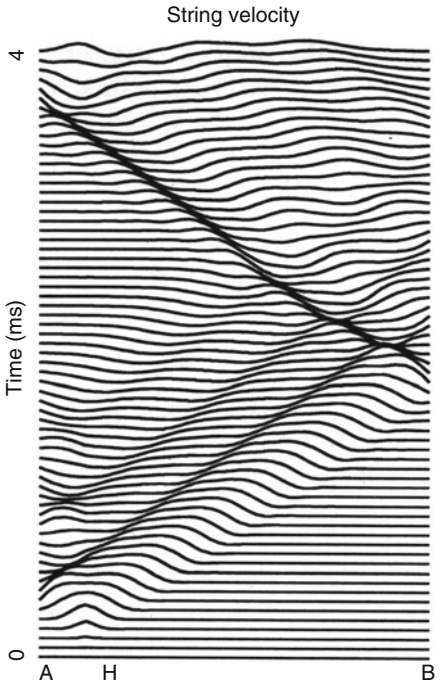

Fig. 3.15 Simulation of the wave propagation on a piano wire just after the hammer impact. The letter H marks the position of the hammer, A is the agraffe, and B is the bridge. For about 1 ms, waves are "trapped" on the shorter side (between A and H). There are then released and follow the main front which propagates towards B. At bridge B, the waves are reflected and their sign changes, according to [10]

Consider now the complete structure, composed of N points. For each action component at a given point j, denoted $F_{j|l}$, a motion is induced at any point i. If $V_{i|k}$ represents one component of this motion, we define for the pair $(V_{i|k}, F_{j|l})$ the *transfer admittance*:

$$Y_{ij|kl} = \frac{V_{i|k}}{F_{j|l}} \quad \text{with} \quad 1 \leq i, j \leq N \quad \text{and} \quad 1 \leq k, l \leq 6 \,. \tag{3.99}$$

In total, we obtain for the *transfer admittance matrix* a group of $6N \times 6N$ coefficients such as $Y_{ij|kl}$ to characterize the structural response to external stimuli.

As an application of the concept of transfer admittance, one can think of the sympathetic excitation of the strings of an instrument through the bridge: the point j refers to the attachment point at the bridge of the excited string, while the point i refers to the attachment point of the sympathetic string (see Fig. 3.18). The sympathetic string vibrates if some frequencies of the excitation signal in j are close to eigenfrequencies of string i and, in addition, if the admittance coefficient Y_{ij} at this frequency is sufficiently high and does not correspond, for example, to a vibration node of the bridge at this frequency. The concept of admittance is essential for understanding the behavior of coupled strings in the piano [39] (see Chap. 6).

Notation. In what follows, the indices (k, l) used for designating the components of force and velocity are removed for simplicity. The coefficients of the transfer

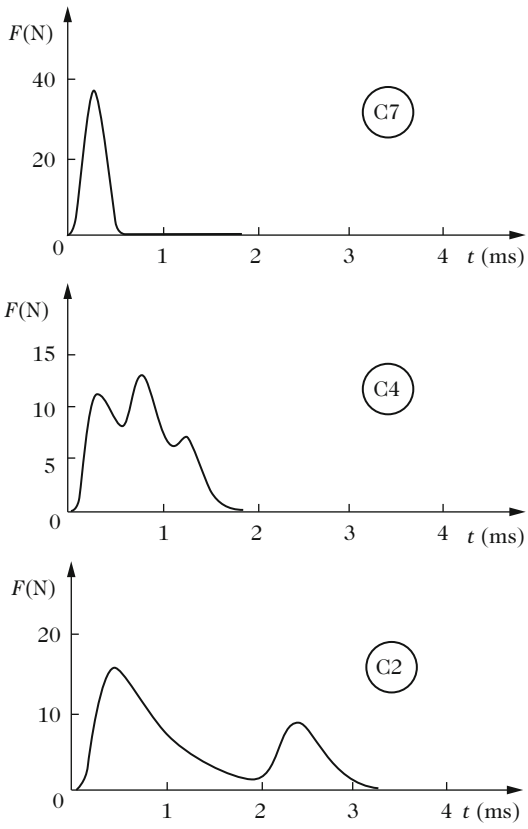

Fig. 3.16 Simulations of the interaction force between hammer and string. (*Top*) String C7 (2093 Hz); (*Middle*) String C4 (262 Hz); (*Bottom*) String C2 (65.4 Hz). The amplitude modulations of the envelope are due to the waves returning from the agraffe to the hammer, according to [11]

admittance matrix are written Y_{ij}, which can be reduced to Y_{ii} (or simply to Y_i through index contraction) in the case of the admittance coefficients at the driving-point. Emphasis is put on force and translation velocity, though the results can be generalized to moments and rotations.

The frequency behavior of the transfer admittance coefficients Y_{ij} are now examined. The force excitation is located at the coordinate x_j. The displacement at a given point x_i on the structure is: $\xi_i = \sum \Phi_n(x_i) q_n(t)$. To be consistent with the notation used for a continuous medium, we write: $\xi(x_i) = \xi_i, f(x_j) = f_j$. The corresponding vector component is written $\Phi_n(x_j)$. According to (3.18), we derive: $f_n = \Phi_n(x_j) f(x_j)$. Equation (3.19) can be rewritten as:

$$\ddot{q}_n(t) + \omega_n^2 q_n(t) = \frac{\Phi_n(x_j) f(x_j)}{m_n} \,. \tag{3.100}$$

In the frequency domain (using the convention of writing the variables in capital letters), the generalized displacements $Q_n(\omega)$ are

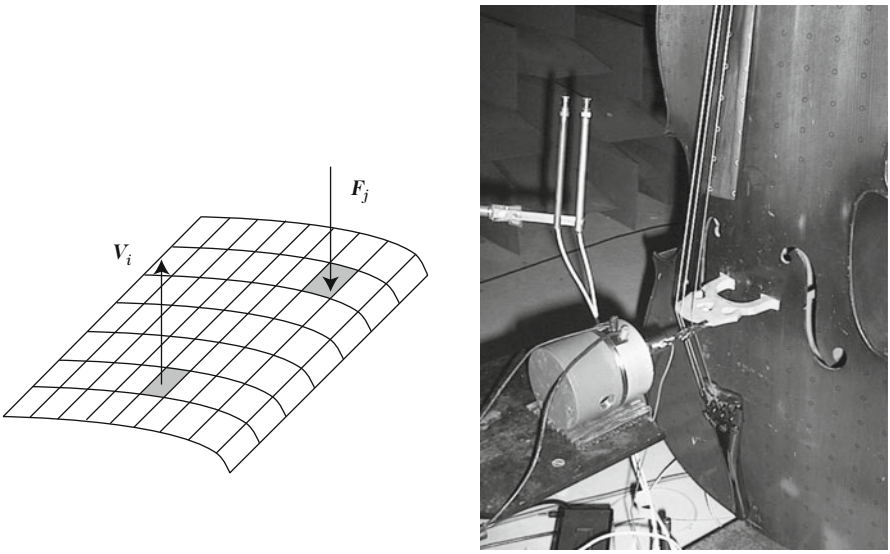

Fig. 3.17 (*Left*) Transfer admittance for a structure with N degrees of freedom. For each pair of points $1 \leq i,\ j \leq N$, the transfer admittance $Y_{ij|kl}$ is the ratio between the velocity component $V_{i|k}$ at point i and the force component $F_{j|l}$ at point j. (*Right*) Vibratory and acoustic analysis of a cello. We note on the cello soundboard the presence of circles marking positions of excitation or response in modal analysis experiments (© A. Garcia, CNAM)

$$\left(\omega_n^2 - \omega^2\right) Q_n = \frac{\Phi_n(x_j) F(x_j)}{m_n} \,. \tag{3.101}$$

Through modal projection, the displacement at point x_i is

$$\Xi(x_i) = \sum_{n=1}^{N} \frac{\Phi_n(x_i)\Phi_n(x_j)}{m_n\left(\omega_n^2 - \omega^2\right)} F(x_j), \tag{3.102}$$

where N corresponds to the number of discrete points on the structure (and thus to the number of modes). The quantity $\Xi(x_i)$ in Eq. (3.102) represents the shape of the structure (commonly referred to as the *Operating Deflection Shape or ODS*) for a forced excitation with frequency ω located at point x_j, from which the transfer admittance between points x_i and x_j is derived:

$$Y_{ij}(\omega) = j\omega \sum_{n=1}^{N} \frac{\Phi_n(x_i)\ \ \Phi_n(x_j)}{m_n\left(\omega_n^2 - \omega^2\right)} \,. \tag{3.103}$$

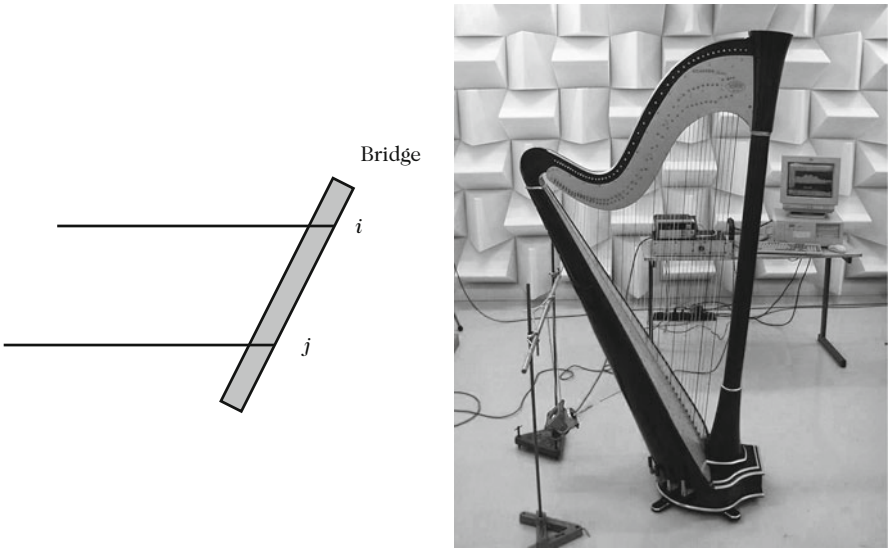

Fig. 3.18 (*Left*) Excitation of sympathetic strings. Several strings which have one end fixed to a moving bridge are likely to vibrate in sympathy. Such a phenomenon requires two conditions: the transfer admittance between i and j should not be zero, and the strings must have at least one eigenfrequency in common. (*Right*) The harp is an example of instrument where sympathetic vibrations are observed, because of the coupling of the strings through the mounting bar located on the axis of the soundboard [24]

N.B. *The symbol j in the previous expression refers to the complex root of unity, and should not be confused with the index "$_j$" which appears in the spatial coordinates and the mechanical variables.*

The driving-point admittance at point x_i is

$$Y_i(\omega) = j\omega \sum_{n=1}^{N} \frac{\Phi_n^2(x_i)}{m_n \left(\omega_n^2 - \omega^2\right)} \,. \tag{3.104}$$

Note Both expressions (3.103) and (3.104) were obtained within the framework of the modal theory for conservative systems, i.e., with no damping. In practice, it is more realistic if account is taken of dissipation in the structure. It will be shown in Chap. 5 that, under some particular assumptions, the modal shapes remain unchanged in the presence of damping, so that one can write:

$$Y_{ij}(\omega) = j\omega \sum_{n=1}^{N} \frac{\Phi_n(x_i)\ \ \Phi_n(x_j)}{m_n \left(\omega_n^2 + 2j\zeta_n\omega_n\omega - \omega^2\right)} \,, \tag{3.105}$$

where ζ_n is a one-dimensional modal damping coefficient, with the assumption $\zeta_n \ll 1$. As a result, the admittance can be considered as being a sum of damped SDOF oscillators (see Chap. 2).

3.4.8.1 Frequency Analysis of Admittances

The modulus of $Y_{ij}(\omega)$ reaches its maximum at frequencies close to the eigenfrequencies of the structure. These maxima are sometimes difficult to detect, especially if the modes are closely spaced in frequency, and with significantly different amplitudes. The imaginary part of the admittance vanishes for frequencies equal to the eigenfrequencies of the structure, and the slope of the phase is maximum (see Figs. 3.19 and 3.20). In the presence of modal damping, a better accuracy is often obtained by using the imaginary part (rather than the magnitude) to determine the eigenfrequencies from experimental admittance measurements.

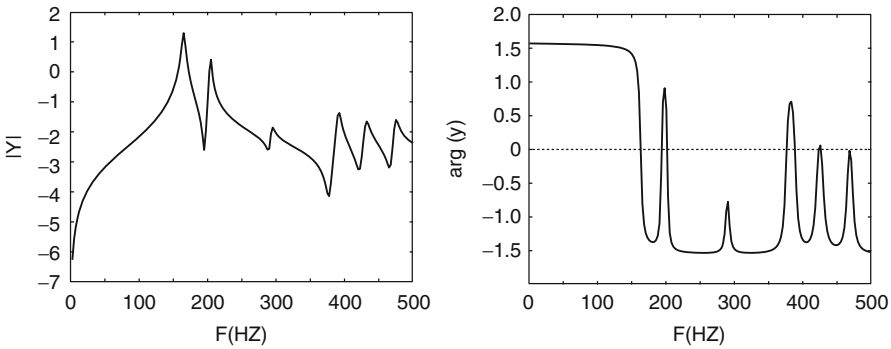

Fig. 3.19 Example of a typical admittance, highlighting the dependence of magnitude and phase on frequency

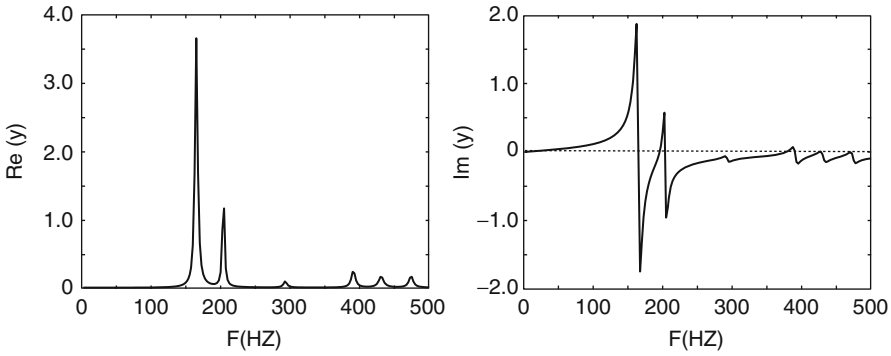

Fig. 3.20 Example of a typical admittance, highlighting the dependence of real and imaginary parts on frequency

- When $\omega \simeq \omega_n$, the main term of $Y_{ij}(\omega)$ is equal to $j\omega \dfrac{\Phi_n(x_i)\ \Phi_n(x_j)}{m_n\left(\omega_n^2 - \omega^2\right)}$.
- When $\omega \gg \omega_n$, the coefficients become

$$Y_{ij} \simeq j\omega \sum_{l>n} \frac{\Phi_l(x_i)\ \Phi_l(x_j)}{-m_l\omega^2} \simeq \frac{1}{j\mathsf{M}\omega} \quad \text{with} \quad \frac{1}{\mathsf{M}} = \sum_{l>n} \frac{\Phi_l(x_i)\ \Phi_l(x_j)}{m_l} \,. \tag{3.106}$$

  All modes with a rank higher than a given value n play the role of a mass M whose value depends on the modal masses and modal shapes at points x_i and x_j. The value of M depends on rank n.
- Similarly, considering the modes with rank lower than n, we find

$$Y_{ij} \simeq j\omega \sum_{l<n} \frac{\Phi_l(x_i)\ \Phi_l(x_j)}{m_l\omega_l^2} \simeq \frac{j\omega}{\mathsf{K}} \quad \text{with} \quad \frac{1}{\mathsf{K}} = \sum_{l<n} \frac{\Phi_l(x_i)\ \Phi_l(x_j)}{m_l\omega_l^2} \,. \tag{3.107}$$

  The contribution of these modes is equivalent to a stiffness K. In summary, in the vicinity of a given mode n, the transfer admittance can be written approximately as:

$$Y_{ij}(\omega) \simeq j\omega \frac{\Phi_n(x_i)\ \Phi_n(x_j)}{m_n\left(\omega_n^2 - \omega^2\right)} + \frac{j\omega}{\mathsf{K}} + \frac{1}{j\mathsf{M}\omega} \,. \tag{3.108}$$

  In summary, Eq. (3.108) shows that one cannot generally consider the term of rank n only in the expansion of Y_{ij}; it is also necessary to take both the mass and stiffness residues M and K into account. These two terms represent the influence of the other modes in the vicinity of the n-th mode.

3.4.9 *Strings of Bowed Instruments*

Bowed strings are either single wires (like the *E*-string of a modern violin) or wrapped strings, where a central wire core is overwound with some form of fine wire. Pickering [29] and Schumacher [34] investigated the mechanical behavior of strings for bowed instruments in detail. In the case of wrapped strings, the core can either be made of a monofilament (steel, tungsten or aluminum) or made of many threads (generally nylon, but sometimes also steel). The winding is a metallic ribbon or a thread (different kinds of aluminum, silver, copper, or tungsten alloys) twisted around the core.

Each string of the instrument is stretched with tension T during the initial tuning. During normal playing, the length L is changed for each note. These two parameters will be considered as constant in what follows, although this is not totally true in

practice. In fact, the use of vibrato (a modulated motion of a finger, resulting in four to eight oscillations per second) affects both the actual length of the string and its tension, and probably also the mobility at the bridge. The amplitude of this motion varies during a note interval, however, on average, it results in an increase in tension.[13]

Three main types of waves are observed in a vibrating string.

- Longitudinal waves can generally be ignored in the motion of bowed strings.
- (Transverse) bending waves are predominant. Since the main component of the bowed string motion occurs in the plane formed by the direction Ox of the string at rest and the direction Oy of the bow velocity, only this polarization plane will be considered for transverse waves in the following sections.
- Torsional waves involve the angular displacement $\psi(x,t)$ of each section of the string, with regard to the string axis Ox. Since the bow excites the string at its outer surface, these waves are always present in a bowed string.

3.4.9.1 Bending Waves

When a string is deflected from its rest position, it tends to return back under the combined effects of two restoring forces oriented in the Oy-direction: one due to the tension T and the other due to the intrinsic stiffness of the string. The restoring force on a portion of string of length dx is $T\dfrac{\mathrm{d}^2\xi}{dx^2}$, where ξ is the displacement along Oy. For a single string with Young's modulus E and geometric moment of inertia of a cross-section I_g, the restoring force due to the finite elasticity of the string is $-EI_g\dfrac{\mathrm{d}^4\xi}{dx^4}$ (see Chap. 1).

Bowed strings are only single wires; most often they present very complex wrapped structures. However, assuming that the structure remains invariant during the deformation (which means that there is no aggregation of the threads in the neutral plane, for example), we can homogenize the cross-section of the string and consider an equivalent single string. The stiffness force then keeps the same formal expression $-\langle EI_g\rangle\dfrac{\mathrm{d}^4\xi}{dx^4}$, where $\langle EI_g\rangle$ is an equivalent bending modulus. For a string with linear density[14] ϵ, the equation of motion becomes

$$-\langle EI_g\rangle\frac{\mathrm{d}^4\xi}{dx^4}+T\frac{\mathrm{d}^2\xi}{dx^2}-\epsilon\frac{\mathrm{d}^2\xi}{dt^2}=0 \quad . \tag{3.109}$$

This equation is dispersive because of the presence of the stiffness term (see the example of a prestressed bar in Sect. 3.5.1.4). The dispersion is low if the

[13] The period of a vibrato is typically 125 ms whereas the largest period of a violin note is only 5 ms (up to 25 ms for the double bass). In view of this duration, it is justified to consider the *average* tension increase in the string.

[14] ϵ is denoted ρS for a homogeneous single wire string.

perturbation term $\varepsilon = \langle EI_g \rangle / TL^2$ is small compared with unity (see Eq. 3.138), which is the case for bowed instruments. The important point here is that the eigenfrequencies of the string are inharmonic. However, for a bowed string, we will see in Chap. 11 that the motion is composed of self-sustained oscillations and is thus quasi-periodic. As a consequence, the components of the bowed string motion *do not coincide* with the eigenfrequencies of the string. In contrast, in the case of free oscillations, like those resulting from a "pizzicato" pluck, the sound spectrum consists of the eigenfrequencies predicted by Eq. (3.138).

One effect of string end mobility is a modification of the string's eigenfrequencies compared with the case where the ends are rigidly fixed (see Sect. 3.4.5). To a first-order, the relative change is equal to (see Eq. 6.54):

$$\frac{\delta f_n}{f_1} \approx \frac{jZ_{c,T}Y}{\pi}, \tag{3.110}$$

where $Z_{c,T}$ is the characteristic impedance of the bending waves and Y the mobility at one end of the string (either in $x = 0$ or $x = L$) assuming that the other end is fixed. The end mobility usually has a reactive component which modifies the eigenfrequencies and a dissipative component which introduces damping in the eigenmodes or, equivalently, a finite width in the resonance curve.

During the coupling with the bow, a transverse string mode can be excited if the inharmonicity resulting from both the stiffness and finite end mobility remains lower than the width of the resonance curve related to dissipation.

3.4.9.2 Torsional Waves

Like the bar of circular cross-section described in Chap. 1, the string has a torsional stiffness GJ, so that the relationship between the moment $\mathscr{M}(x,t)$ exerted on a section and its angular displacement ψ is given by [see Chap. 1, Eq. (1.42)]:

$$\mathscr{M}(x,t) = GJ\frac{\mathrm{d}\psi}{dx}\ . \tag{3.111}$$

The string also has a rotational inertia with regard to its axis, with moment I per unit length. The equation for torsional waves (see Chap. 1, Eq. (1.45)) can then be written as:

$$\frac{\mathrm{d}^2\psi}{dx^2} - \frac{1}{c_R^2}\frac{\mathrm{d}^2\psi}{dt^2} = 0 \quad , \tag{3.112}$$

where the propagation speed c_R is $\sqrt{GJ/I}$. This speed is about five times higher than the propagation speed for transverse waves. Torsional waves have an important intrinsic damping: their associated Q-factor is typically a few tens, an order of

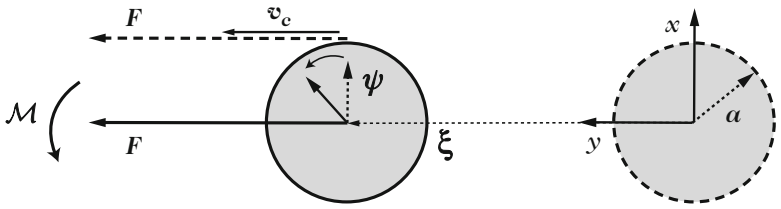

Fig. 3.21 Transverse displacement ξ combined to the rotation ψ of a string section consecutive to a horizontal force F applied at its surface by the bow. *Right*: string at rest; *left*: string in motion

magnitude below that for bending waves [20, 42]. Torsional waves also have a characteristic impedance which links $\mathscr{M}$ and $\dot{\psi}$ for a traveling wave:

$$\mathscr{M} = \pm\sqrt{JGI}\,\dot{\psi}\ . \tag{3.113}$$

Finally, a force F applied at the string's curved outer surface is equivalent to the following combination (see Fig. 3.21):

- a force F applied at the center generating a bending wave and
- a moment $\mathscr{M} = aF$ (where a is the string's radius) which generates the torsional wave $\psi(x,t)$.

The expression of the velocity v_c at the string's surface combines together the torsional and the bending waves:

$$v_c = \dot{\xi} + a\dot{\psi}, \tag{3.114}$$

It is generally more convenient to use the variables (v_c, F) for describing the combination of both traveling waves:

$$v_c = Y_{c,T}F + a^2\frac{F}{\sqrt{JGI}} = Y_c F, \tag{3.115}$$

where

$$Y_c = Y_{c,T} + \frac{a^2}{I\,c_R} \tag{3.116}$$

is the resulting mobility of the string at its surface. In this expression, the characteristic impedance of the torsional waves, seen from the outer curved surface of the string, is

$$Z_R = \pm\frac{F}{a\dot{\psi}} = \frac{I\,c_R}{a^2}. \tag{3.117}$$

The characteristic mobility Y_c will be used to describe the dynamics of the string in Chap. 11.

3.5 Application to Percussion Instruments

Percussion instruments are characterized by a short excitation, followed by free oscillations. In the linear range, the spectral content of the sound during decay is composed of the eigenfrequencies of the excited system. In the first chapter of this book, the basic equations describing the vibrations of elementary structures such as bars, plates, membranes, and shells were presented. A number of percussion instruments are made up of such structures. In Chap. 1, the main impact mechanisms were also described. Using the general properties of modes, we are now able to apply these results to percussive instruments.

3.5.1 Vibration of Beams

Beam models are well suited to the description of tuned mallet percussion instruments with keyboard such as the xylophone, vibraphone, marimba, glockenspiel, etc. For these instruments, the bending transverse vibrations are dominant, and deserve careful attention. However, other modes, including torsional modes, can also be excited. This is particularly true in the upper frequency range of these instruments, when the length of the beam becomes comparable to the other dimensions, and therefore treating the beam as a "slender solid" is no longer valid.[15]

In this section we restrict ourselves to the case of transverse bending vibrations. We first examine the analytical reference solution provided by the case of bars with constant cross-section. We then study the case of bars of variable cross-section, which better correspond to real instruments. Finally, the particular case of prestressed bars allows us to establish a comparison with the transverse vibrations of strings discussed in Sect. 3.4.

As shown in Chap. 1, the basic equation describing the transverse bending vibrations of bars, assuming Euler–Bernoulli assumptions and isotropic material, is written:

$$\frac{\partial^2}{\partial x^2}\left(EI(x)\frac{\partial^2 y}{\partial x^2}\right) + \rho(x)S(x)\frac{\partial^2 y}{\partial t^2} = 0\,, \tag{3.118}$$

where $y(x,t)$ is the transverse vertical displacement (in the $\boldsymbol{e}_y$ direction). The eigenmodes $y(x,t) = \Phi(x)\cos\omega t$ are the sinusoidal solutions of (3.118) which satisfy the equation:

[15] In musical acoustics, the word *bar* is often used to designate xylophone beams. Both terms are used in this book. In structural dynamics, the term *beam* is used to designate slender solids in bending regime, while the term *bar* is used in the context of longitudinal vibrations. We do not make such a distinction here.

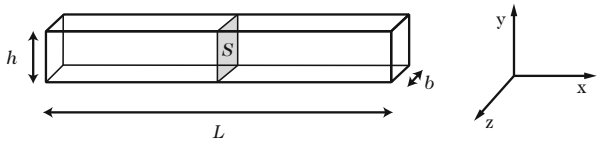

Fig. 3.22 Geometry of a bar with a constant cross-section

$$\frac{d^2}{dx^2}\left(EI(x)\frac{d^2\Phi}{dx^2}\right) - \omega^2\rho(x)S(x)\Phi = 0\,. \tag{3.119}$$

Equation (3.119) cannot be solved analytically, except in a small number of cases such as a bar of constant cross-section, discussed in Sect. 3.5.1.1 below. For variable cross-section bars, we must use approximate resolution techniques (see Sect. 3.5.1.2).

3.5.1.1 Free-Free Bars of Constant Cross-Section

Consider the reference case of an homogeneous, isotropic bar of length L, width b, thickness h, constant cross-section $S = bh$, whose moment of inertia with respect to the neutral plane at $z = h/2$ (see Fig. 3.22) is $I = bh^3/12$.

In this case, Eq. (3.118) reduces to:

$$EI\frac{\partial^4 y}{\partial x^4} + \rho S\frac{\partial^2 y}{\partial t^2} = 0\,. \tag{3.120}$$

Searching eigensolutions of the form $y(x,t) = \Phi(x)\cos\omega t$ leads to [19]:

$$\Phi(x) = A\cosh kx + B\sinh kx + C\cos kx + D\sin kx$$
$$\text{with}\quad k = \tfrac{\omega}{v}\quad\text{where}\quad v = \sqrt{\omega}\sqrt[4]{\tfrac{EI}{\rho S}}\,. \tag{3.121}$$

This expression shows that the *phase velocity* v of the bending waves varies as the square root of the angular frequency ω. The waves are therefore dispersive, the high frequencies propagating faster than the low frequencies. The associated dispersion equation is

$$EIk^4 - \rho S\omega^2 = 0, \tag{3.122}$$

from which we obtain v as a function of wavenumber k:

$$v = \frac{\omega}{k} = k\sqrt{\frac{EI}{\rho S}}\,. \tag{3.123}$$

However, in terms of energy transportation, the appropriate velocity to consider is not the phase velocity, but the group velocity (see, for example, [21]). For a "wave packet" localized in time, the group velocity is the velocity of the envelope, which can be calculated by:

$$v_g = \frac{\partial \omega}{\partial k} = 2k\sqrt{\frac{EI}{\rho S}} = 2v = 2\sqrt{\omega}\sqrt[4]{\frac{EI}{\rho S}}\,. \tag{3.124}$$

The group velocity here is twice the phase velocity. This result reveals a paradoxical phenomenon, namely that the group velocity of elastic bending waves in the bar tends to infinity with frequency. This is in disagreement with the basic laws of physics since if would mean that some bending waves could propagate faster than light! This apparent paradox is a result of the simplified model of Euler–Bernoulli which ignores the effects of rotational inertia of the bar and the shear of the cross-sections. Introducing these two corrections into the bar model (Timoshenko model [18]), shows that the velocity of the bending waves actually varies as $\sqrt{\omega}$ at low frequencies and then tends to a constant asymptotic value as the frequency increases, which is more realistic (see Fig. 3.23).

Continuing the calculation, we introduce the free boundary conditions (Fig. 3.24), which amount to nullifying moments and forces exerted by the external environment on the ends of the bar (see Chap. 1), which yields

$$\begin{aligned} &\frac{\partial^2 y}{\partial x^2}(0,t) = \frac{\partial^2 y}{\partial x^2}(L,t) = 0, \\ \text{and}\quad &\frac{\partial^3 y}{\partial x^3}(0,t) = \frac{\partial^3 y}{\partial x^3}(L,t) = 0\,. \end{aligned} \tag{3.125}$$

Finally, the eigenfrequency equation for a bar of constant cross-section free at both ends (see Fig. 3.26) is

$$\cos kL \cosh kL = 1\,. \tag{3.126}$$

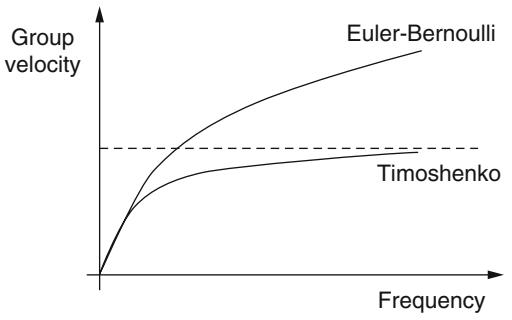

Fig. 3.23 Group velocity of bending waves in a bar, for different models

Fig. 3.24 On tuned keyboard percussion instruments, the "free-free" boundary conditions are obtained by attaching the bars together with a light and flexible cord. The attachment points of the cord on the bar are approximately located at the position of the nodes of the fundamental mode in order to minimize damping. We see on this figure the example of a balafon or African xylophone

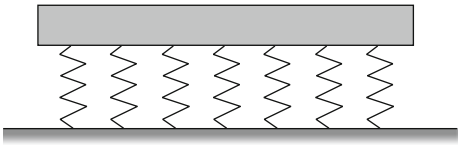

Fig. 3.25 Xylophone bar with its suspension

Note 1: In (3.126), the solution $k = 0$ does not hold: it would correspond to the case where the free bar goes to infinity after the impact. Imagine, for example, striking a bar with a hockey stick on a frozen lake: it will take a rigid body motion made of the combination of translation and rotation, and you will have to run far away to recover it!

Note 2: In practice, the boundary conditions are satisfied by flexible suspensions.[16] These suspensions, combined with the total mass of the bar, provide an extra rigid body mode (see Sect. 3.4.1.1). This mode usually has an eigenfrequency of a few Hz, which is very low as compared with the first eigenfrequency of the transverse motion (see Fig. 3.25).

The graphical resolution of Eq. (3.126) in Fig. 3.26 shows that the roots are such that $k_n L \simeq (2n + 1)\pi/2$. From the dispersion equation (3.122), we derive the eigenfrequencies f_n (in Hz):

[16]The arrangement of bars of ascending pitch is, for example, maintained by a thin cord which passes through all bars.

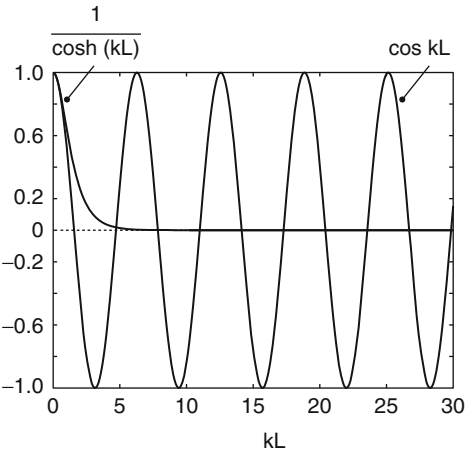

Fig. 3.26 Graphical solution of the eigenfrequency equation for a free homogeneous bar of constant cross-section: the solutions are found at the intersections of the curves $\cos kL$ and $\frac{1}{\cosh kL}$

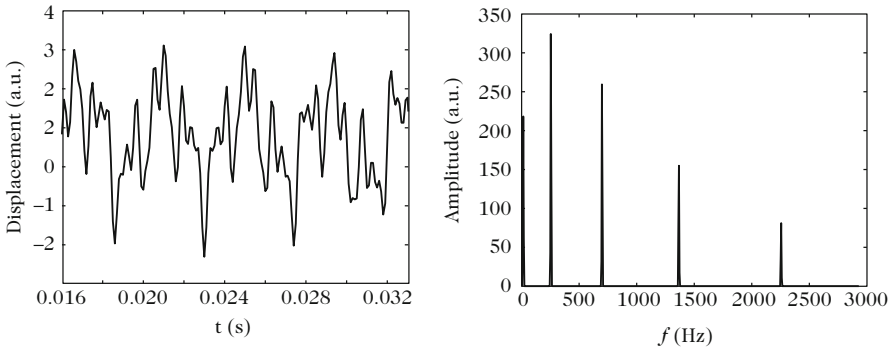

Fig. 3.27 Waveform and amplitude spectrum for a bar of constant cross-section. The waveform is not periodic and the spectral components are not integer multiples of the fundamental

$$f_n \simeq \sqrt{\frac{EI}{\rho S}} \frac{\pi}{8L^2} \left[3^2, 5^2, 7^2, \ldots, (2n+1)^2\right] . \tag{3.127}$$

Unlike for the case of an ideal string, the bending eigenfrequencies for a bar of constant cross-section are inharmonic, i.e., they are not integer multiples of a fundamental. This property is apparent in Fig. 3.27 which shows the amplitude spectrum for the vibration of a bar of constant cross-section. On the same figure, an extra peak close to zero (a few Hertz) can be seen which corresponds to the suspension resonance of the bars. This resonance, which is not predicted by Eq. (3.126), does not produce any sound.

From a musical point of view, the major shortcoming of an inharmonic spectrum is that the perceived pitch is not well defined. For this reason, the bars are cut on their lower side. The eigenfrequencies of bars with an undercut can be calculated from Eq. (3.119). In this case, there is no analytical solution and one has to use

numerical approximations. It is possible to optimize the width and depth of the cut (while respecting other criteria such as, for example, the non-appearance of torsional vibrations and the elasticity limit of the bar) in order to ensure that the partials of higher rank will be close to multiples of the fundamental.

3.5.1.2 Bars of Variable Cross-Section

The Galerkin method of solving the eigenvalue problem for the bending vibrations in a bar of variable cross-section is now briefly explained [26]. This method applies to conservative and non-conservative problems. It is an approximation method where the eigenmodes $\Phi(x)$ are sought in the form of a finite sum of p terms:

$$\Phi^{(p)}(x) = \sum_{j=1}^{p} a_j \phi_j(x) \,, \tag{3.128}$$

where the functions $\phi_j(x)$ are arbitrary with the restriction that they must fulfill the boundary conditions: they are said to be *kinematically admissible*. Combining Eqs. (3.128) and (3.119), and defining $\lambda^{(p)} = (\omega^2)^{(p)}$ (the approximate eigenvalues of order p), we obtain the *Galerkin's residue*:

$$\mathscr{R}\left[\Phi^{(p)}(x)\right] = \frac{d^2}{dx^2}\left(EI(x)\frac{d^2\Phi^{(p)}}{dx^2}\right) - \lambda^{(p)}\rho(x)S(x)\Phi^{(p)} \,, \tag{3.129}$$

which can be written, given Eq. (3.128):

$$\mathscr{R}\left[\Phi^{(p)}(x)\right] = \sum_{j=1}^{p} a_j \left\{\frac{d^2}{dx^2}\left(EI(x)\frac{d^2\phi_j(x)}{dx^2}\right) - \lambda^{(p)}\rho(x)S(x)\phi_j(x)\right\} \,. \tag{3.130}$$

The functions $\phi_j(x)$ are now used to obtain a *weak formulation* for the eigenvalue problem, i.e., after multiplication by a function ϕ_i and integration over the entire length of the bar:

$$\int_0^L \phi_i(x) \sum_{j=1}^{p} a_j \left\{\frac{d^2}{dx^2}\left(EI(x)\frac{d^2\phi_j(x)}{dx^2}\right) - \lambda^{(p)}\rho(x)S(x)\phi_j(x)\right\} dx = 0 \,. \tag{3.131}$$

The problem is equivalent to searching those coefficients a_j which cancel the residue $\mathscr{R}\left[\Phi^{(p)}(x)\right]$. The formulation (3.131) can then be written as:

$$\sum_{j=1}^{p} k_{ij}a_j - \lambda^{(p)} \sum_{j=1}^{p} m_{ij}a_j = 0 \quad \text{for} \quad i = 1, 2, .., p \,, \tag{3.132}$$

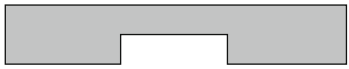

Fig. 3.28 Bar with an undercut

where the mass and stiffness coefficients are given by:

$$k_{ij} = \int_0^L \phi_i(x) \frac{d^2}{dx^2} \left(EI(x) \frac{d^2\phi_j(x)}{dx^2} \right) dx,$$

$$\text{and} \quad m_{ij} = \int_0^L \phi_i(x) \rho(x) S(x) \phi_j(x)\, dx\,. \tag{3.133}$$

Equation (3.132) can be written in matrix form:

$$[\mathbb{K} - \lambda \mathbb{M}]\, \boldsymbol{a} = 0\,, \tag{3.134}$$

where $\boldsymbol{a}$ is a vector of dimension p, and where $\mathbb{K}$ and $\mathbb{M}$ are matrices of dimensions $p \times p$. The method presented is thus equivalent to solving an eigenvalue problem similar to those encountered for discrete systems.

A simple example of a bar of variable cross-section is depicted in Fig. 3.28 which shows a bar with reduced height in its central part. Removing material near the center decreases the inertia (proportional to thickness), but also the stiffness in higher proportion (since the stiffness is proportional to the third power of the thickness), and therefore the eigenfrequencies whose corresponding eigenshapes reach a maximum near the center decrease, which is the case for odd modes. This simple example shows that it is possible to control the spacing of the eigenfrequencies with an appropriate undercut.

3.5.1.3 Application to Xylophone and Keyboard Instruments

In practice, bar shapes similar to the one shown in Fig. 3.28 should be avoided since high internal stress is concentrated near the sharp corners, which weakens the structure. It is preferable to design bar profiles with a high radius of curvature and without slope discontinuities.

Today, the design of bars for keyboard percussion instruments still remains largely empirical. Cutting the bar near its center lowers the frequency f_1 of the first partial, while keeping the frequency f_2 of the second partial approximately constant, and lowering the frequency f_3 of the third partial slightly. Instrument makers usually adjust the ratios $R_1 = f_2/f_1$ and $R_2 = f_3/f_1$. In practice, it becomes difficult to independently adjust the partials of higher rank, and so the focus usually remains on these two parameters only. The depth of the undercut is limited by the resistance of the bar to shocks and by the fact that, if the bar becomes too thin in the center, torsional vibrations might become important. According to Eq. (3.127), the initial values of the two frequency ratios (before starting the undercut) are

$$R_{10} = \frac{25}{9} = 2.754 \quad \text{and} \quad R_{20} = \frac{49}{9} = 5.404\,. \tag{3.135}$$

From experience, it is known that the target for R_1 usually lies between 3 and 4, and between 6 and 10 for R_2. The standard values used by makers are the following:

- $R_1 = 3$ and $R_2 = 6$,
- $R_1 = 4$ and $R_2 = 8$,
- $R_1 = 3$ and $R_2 = 9$,
- $R_1 = 4$ and $R_2 = 10$.

On real tuned mallet percussion instruments, these ratios can only be obtained for the lower notes. In the middle register, the second and third partials are not in harmonic ratio with the fundamental anymore. This is due to the fact that the assumption that a bar behaves as a 1D slender solid is less justified as the length of the bars decreases. Orduña-Bustamante suggests to cutting parabolic profiles in the bars [28]. The idea is to adjust the depth h_c and width x_c of the undercut to obtain appropriate values for R_1 and R_2. This idea has been extended by Doutaut who suggests polynomial profiles of order 4 and 8, enabling a larger range of possible modifications for the eigenfrequencies (see Fig. 3.29) [12].

In order to tune the complete range of bars in a mallet percussion instrument, it is necessary to adjust both the shape of the undercut and the length of the bars. For an instrument with four octaves, the ratio between the higher and the lower fundamental is $f_{\max}/f_{\min} = 2^4 = 16$. Since the eigenfrequencies of the bars vary as the inverse of the square of the length [see Eq. (3.127)], in principle, it might be considered that the length of the bars should be adjusted such that $D = L_{\max}/L_{\min} = 4$. However, measuring actual bar lengths on most real instruments shows that D is close to 3. There are several reasons for this: the first reason is with respect to the playability of the instrument; the player would encounter difficulties in playing on very short bars in the high frequency range. At the other end of the instrument, long bars at low frequencies would be more difficult to produce, would take more space and would use more material. The second reason is linked to manufacturing, because of the constraints associated with the attachment of the bars. Finally, as mentioned

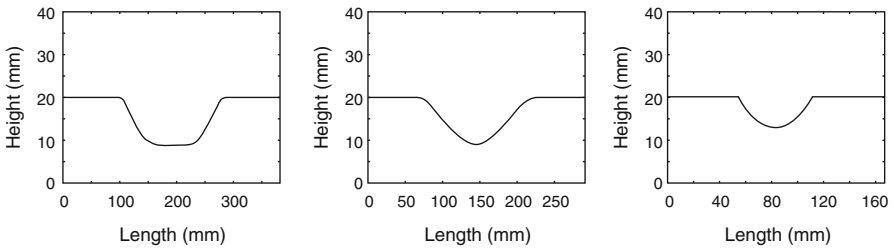

Fig. 3.29 Examples of undercut shapes for xylophone bars. (*Left*) Polynomial of order 8 for bar C4 ($f_1 = 262$ Hz); (*Middle*) Polynomial of order 4 for bar C5 ($f_1 = 524$ Hz; (*Right*) Polynomial of order 2 for bar C7 ($f_1 = 2093$ Hz), according to [12]

above, it is preferable to have longer bars at high frequencies for tuning reasons. In practice, to make a chromatic instrument where fundamental frequencies vary by 6 % from one note to the next, about 5 % of the variations are obtained by modifying the lengths of the bars and the remaining 1 % by adjusting the cuts. Makers tend to start by using the most usable length of bar for the high frequency notes, and then make greater and greater undercuts as they work towards the lower notes.

3.5.1.4 Prestressed Bars and Stiff Strings

Strings of musical instruments are made of elastic materials that have a finite Young's modulus. As a consequence, it is impossible to create any discontinuity of slope by bending the string. This is particularly true for metallic strings, such as piano wires. If such a string is fixed at one end, when undisturbed it remains almost straight, like a bar. Therefore, it is necessary to refine the previous ideal string model, to take both the axial prestress (due to tension T) and bending stiffness into account. The equation that describes the transverse bending vibrations of a stiff string (or, equivalently, of a prestressed bar), assuming an Euler–Bernoulli behavior, becomes

$$\rho S \frac{\partial^2 y}{\partial t^2} = T \frac{\partial^2 y}{\partial x^2} - EI \frac{\partial^4 y}{\partial x^4} \, . \tag{3.136}$$

For a traveling wave of the form $y(x,t) = e^{j(\omega t - kx)}$, we obtain the dispersion equation:

$$\omega^2 = k^2 c^2 \left(1 + \frac{EI}{T} k^2\right) \, . \tag{3.137}$$

For a string of length L, the usual orders of magnitude are such that it is justifiable to define a dimensionless coefficient $\varepsilon = \frac{EI}{TL^2}$, small compared to unity, so that Eq. (3.137) becomes

$$\omega^2 = k^2 c^2 \left(1 + \varepsilon k^2 L^2\right) \, . \tag{3.138}$$

For the case of a stiff string simply supported at both ends, the displacement and moment are both zero at these points, which yields the condition for the wavenumbers:

$$\sin kL = 0 \quad \text{i.e.} \quad k_n L = n\pi \, . \tag{3.139}$$

From Eq. (3.138), the eigenfrequencies of the stiff string are given by:

$$\omega_n \simeq \frac{n\pi c}{L} \left(1 + \varepsilon \frac{n^2 \pi^2}{2}\right) \, . \tag{3.140}$$

Due to bending stiffness, the eigenfrequencies of the stiff string are higher than those of the corresponding ideal string. This difference increases with the rank n of the partial. This property is observed on piano wires [30]. The inharmonicity due to stiffness for the nth-partial of the string is defined as:

$$i_n = \frac{\omega_n - \omega_{no}}{\omega_{no}} , \tag{3.141}$$

where ω_{no} is the angular frequency in the case of no stiffness. The application of this definition to the present case leads to:

$$i_n = \varepsilon \frac{n^2 \pi^2}{2} . \tag{3.142}$$

In real instruments, the inharmonicity due to stiffness should be added to the inharmonicity due to the coupling with the soundboard, as studied in Sect. 3.4.5.

Time Domain: Precursor

For stiff strings, the dispersion equation (3.138) shows that the phase velocity $v_\phi = \omega/k$ and the group velocity $v_g = \frac{d\omega}{dk}$ are both monotonic increasing functions of frequency. In the time domain, rapidly varying oscillations preceding steep wavefronts can be seen on force waveforms (see Fig. 3.30). These oscillations were called "precursors" by Cuesta and Valette [38]. These authors also highlighted the modifications of the precursor due to amplitude nonlinearity (see Chap. 8) and their perceptual significance.

3.5.2 *Vibrations of Membranes In Vacuo*

A similar distinction can be made for 2D systems as it has been previously made for strings and bars. In what follows, an *ideal membrane* refers to a thin structure, i.e., whose thickness is small compared with the other dimensions, and where the elastic

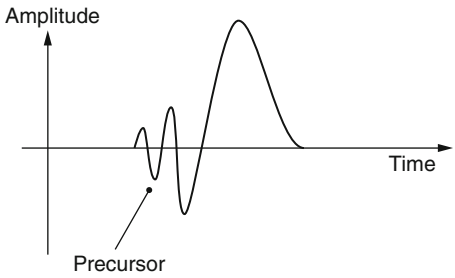

Fig. 3.30 Precursor due to stiffness in linear regime

restoring forces are due to prestress, i.e., to a surface tension applied at its periphery. Conversely, a *plate* is a thin, two-dimensional structure where the restoring forces are due to the intrinsic elasticity of the material. As for strings, real membranes have a nonzero modulus of elasticity. Finally, we also find prestressed plates in musical acoustics, such as the soundboard of a piano. For almost all string instruments, the body of the instrument is prestressed by the tension of the strings. In membranes, in addition, the presence of both the surrounding air and the cavity influences the vibrations. This is due to both the large surface in contact with the fluid and the small thickness of the membrane. In this section, only the case of membrane vibrations in vacuo will be addressed, keeping in mind that this reference case has no practical interest in musical acoustics. However, it will be used in Chap. 14 for building a kettledrum model.

3.5.2.1 Transverse Free Vibrations of a Circular Membrane

Membranes are used in percussion instruments (timpani, drums, bass drum, etc.) and in a number of string instruments (banjo [31], African kora, etc.). A circular geometry is usually preferred so as to obtain homogeneous tension across the membrane (Fig. 3.31). Membranes are usually excited by impact and therefore the oscillations are free after the mallet (or stick) has left the membrane. The discussion here is restricted to free oscillations. Assuming small displacements (which might not be justified during the excitation phase in the case of strong impacts), one can assume that the free transverse displacement $z(r, \theta, t)$ of a membrane in vacuo with surface density σ (in $\mathrm{kg\,m^{-2}}$) and tension per unit length τ (in $\mathrm{N\,m^{-1}}$) is described by the 2D wave equation (see Chap. 1):

$$\sigma \frac{\partial^2 z}{\partial t^2} = \tau \Delta z = \tau \left[\frac{\partial^2 z}{\partial r^2} + \frac{1}{r} \frac{\partial z}{\partial r} + \frac{1}{r^2} \frac{\partial^2 z}{\partial \theta^2} \right] . \tag{3.143}$$

A standard method of solving Eq. (3.143) is to use separation of variables [21]. A condition of zero displacement at the edge $z(r = a, \theta, t) = 0$ is imposed. In real instruments (in a kettledrum, for example), energy losses occur at the edge of the membrane because of both the presence of absorbing material (such as rubber) and the transmission of vibrations to the kettle. Such dissipation will be ignored in this chapter. For an ideal circular membrane, the transverse displacement can be written as [21]:

$$\begin{aligned} z(r, \theta, t) = \sum_{m=1}^{\infty} \Bigg\{ & \sum_{n=0}^{\infty} Z_{mn}(r, \theta) \left(A_{nm} \cos \omega_{mn} t + B_{nm} \sin \omega_{mn} t \right) \\ & + \sum_{n=1}^{\infty} \tilde{Z}_{mn}(r, \theta) \left(\tilde{A}_{nm} \cos \omega_{mn} t + \tilde{B}_{nm} \sin \omega_{mn} t \right) \Bigg\} . \end{aligned} \tag{3.144}$$

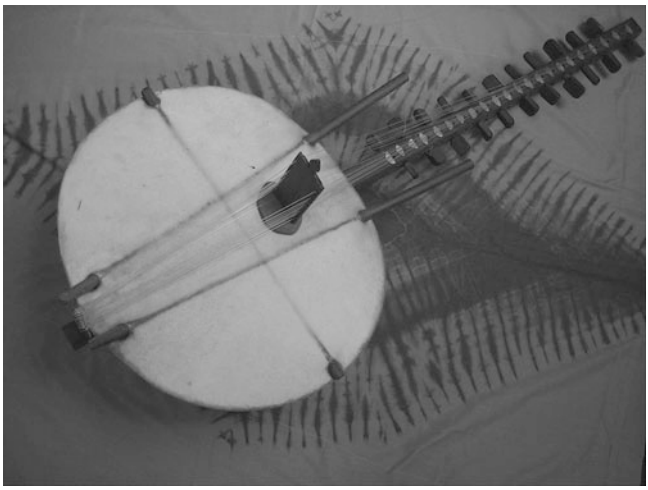

Fig. 3.31 Kora (African harp). The string vibrations are transmitted to a skin (or membrane) coupled to a cavity (a gourd) with a hole on the back

In Eq. (3.144), the eigenshapes of the membrane are given by:

$$Z_{mn}(r,\theta) = J_n(\beta_{mn} r)\cos n\theta \quad \text{and} \quad \tilde{Z}_{mn}(r,\theta) = J_n(\beta_{mn} r)\sin n\theta \,, \tag{3.145}$$

where the functions J_n are the *Bessel functions of the first kind of order n* [1]. Indices m and n correspond to the number of nodal circles and diameters, respectively (see Fig. 3.32). The discrete values of the wavenumber β_{mn} are determined by the boundary conditions at the edge. For a fixed edge, we get

$$J_n(\beta a) = 0 \,. \tag{3.146}$$

For each value of n, we obtain an infinite series β_{mn} of roots of Eq. (3.146). For $n = 0$, for example, we find that $J_0(\beta a) = 0$ yields the solutions $\beta_{m0} a = 2.405,\ 5.520,\ 8.654,\ 11.792,\ 14.931, \ldots$. Similarly, the roots of $J_1(\beta a) = 0$ are given by $\beta_{m1} a = 3.832,\ 7.016,\ 10.173,\ 13.324,\ 16.471, \ldots$.

The first nodal circle ($m = 1$) corresponds to the edge of the membrane. The *symmetrical* modes correspond to the cases where $n = 0$, i.e., with no nodal diameter. In these cases, only the shapes of type $Z_{mn}(r,\theta)$ remain. These modes are excited for a membrane struck near its center. In all other cases, we get twin modes with the same dependence with regard to r but which differ from each other by an angular shift equal to $\pi/2n$. The modes $m1$ are strongly excited when the player strikes near the edge, and are the most important from a musical point of view (see Chap. 14). The eigenfrequencies ω_{mn} are derived from the 2D wave equation (3.143):

$$\omega_{mn} = c\beta_{mn} \quad \text{where} \quad c = \sqrt{\frac{\tau}{\sigma}} \,. \tag{3.147}$$

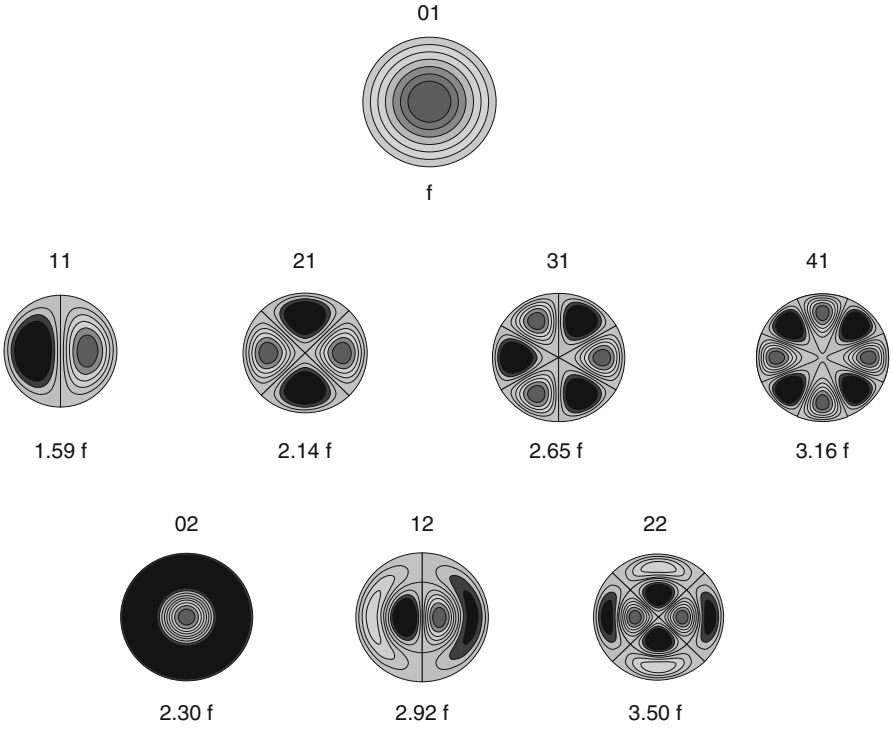

Fig. 3.32 Modal shapes of a circular membrane in vacuo. Each mode is designated by *nm* where *n* is the number of nodal diameters and *m* the number of nodal circles. The corresponding eigenfrequencies are indicated below each shape

In contrast to ideal strings, the eigenfrequencies of a membrane in vacuo are not harmonically related. We will see in Chap. 14, however, that the first modes of the $m1$ family can become almost harmonic under the combined loading effects of surrounding air and cavity. As a consequence, in this situation, a defined pitch can be produced when the membrane is struck near the edge.

3.5.2.2 Modal Density of a Membrane

The transverse vibrations of a membrane in vacuo can be viewed as a 2D generalization of the vibrations of ideal strings. One main difference between these two systems lies in the *modal density* (or number of modes per Hz) observed in their respective spectra.

In this book, we will have several opportunities to discuss the concept of modal density. This quantity influences linear and nonlinear couplings, acoustic radiation, and the statistical representation of vibration phenomena at high frequencies. The modal density of an ideal string stretched between two rigid supports is compared below with the modal density of a rectangular membrane rigidly fixed

at its edges. The rectangular geometry is chosen here only for the sake of simplicity, but the results obtained can be generalized to other geometries. We start by calculating the number of modes $N(f)$ with eigenfrequencies lower than a given frequency f. On a wavenumber scale, the successive modes of a string are equally spaced with an interval equal to π/L. Therefore we have

$$N(f) = \frac{k}{\frac{\pi}{L}} = \frac{2Lf}{c} . \tag{3.148}$$

The modal density is, by definition:

$$D(f) = \frac{dN}{df} = \frac{2L}{c} = \frac{1}{f_1} . \tag{3.149}$$

We find that the number of modes per Hz for an ideal string is equal to the inverse of the fundamental, which is a fairly obvious result. A similar method is now used for a rectangular membrane of length L_x and width L_y. The eigenfrequencies can be obtained by the method of separation of variables. The wavenumbers are now given by:

$$k_{mn} = \sqrt{k_m^2 + k_n^2} = \sqrt{\frac{m^2\pi^2}{L_x^2} + \frac{n^2\pi^2}{L_y^2}} \quad \text{with} \quad m, n \geq 1 . \tag{3.150}$$

In the k-plane, each discrete wavenumber k_{mn} with components (k_m, k_n) is represented by a vector of origin O and whose end is one of the nodes of the mesh with spatial steps $\pi/L_x, \pi/L_y$ (see Fig. 3.33). The number $N(f)$ is obtained by dividing the area of the quarter circle of radius k by the area of one element of the mesh:

$$N(f) = \frac{\pi}{4}\frac{4\pi^2 f^2}{c^2}\frac{L_x L_y}{\pi^2} = \pi\frac{Sf^2}{c^2}, \tag{3.151}$$

where S is the membrane surface area. We derive, in turn, the modal density:

$$D(f) = \frac{dN}{df} = \frac{2\pi S}{c^2} f . \tag{3.152}$$

The modal density of a membrane is proportional to the frequency. We will see in Chap. 5 that, for timpani membranes and for drumheads, the damping also increases with frequency. This leads to a modal overlap, so that it is not possible to discriminate the modes anymore. The spectrum becomes almost continuous.

3.5.3 Transverse Vibrations of Thin Plates

Flat plates can be viewed as two-dimensional bars, the third dimension (thickness) being considered as small compared with length and width. A piano (or a guitar)

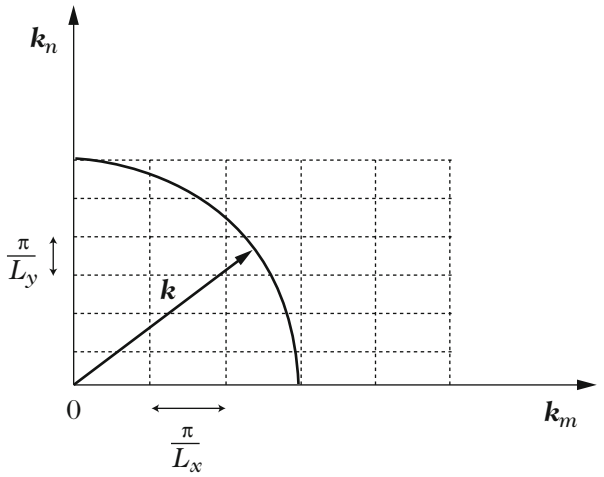

Fig. 3.33 Determining the number of modes and modal density for a two-dimensional system

soundboard is fairly well represented by a plate model. This is also the case for other string instruments, such as harps or lutes. Freely suspended metallic plates can also be used as percussion instruments [33].

In what follows, the transverse plate displacement is assumed to be small enough so that the equation of motion is linear. The thickness is also assumed to be small and the frequency range under study is such that transverse shear and rotational inertia can both be ignored. The transverse vibrations of the plates are then described by the Kirchhoff–Love model (see Chap. 1). This model is a generalization of the Euler–Bernoulli model (previously introduced for bars) to the case of plates.

The modes of simply supported rectangular plates are briefly reviewed below, in the context of musical acoustics. Emphasis is put on orthotropic plates, since most soundboards of string instruments are made of wood. Isotropic plates are thus considered as limiting cases. The effects of boundary conditions are discussed. As for membranes, we limit ourselves to the case of plates in vacuo. The structural-acoustic coupling between vibrating plate and air will be studied in Chap. 13.

3.5.3.1 Simply Supported Rectangular Orthotropic Plates

For a homogeneous orthotropic plate in Cartesian coordinates, with the axes oriented in the principal directions of orthotropy, and under Kirchhoff–Love assumptions, the equation that describes the transverse bending displacement w is (see Chap. 1):

$$\rho_p h \frac{\partial^2 w}{\partial t^2} + D_1 \frac{\partial^4 w}{\partial x^4} + (D_2 + D_4) \frac{\partial^4 w}{\partial x^2 \partial y^2} + D_3 \frac{\partial^4 w}{\partial y^4} = 0 \,. \tag{3.153}$$

For a simply supported rectangular plate of dimensions a and b, the displacement and bending moment are zero at the edges:

$$\begin{aligned} w(0,y,t) = w(a,y,t) = w(x,0,t) = w(x,b,t) = 0 \\ \mathscr{M}_x(0,y,t) = \mathscr{M}_x(a,y,t) = \mathscr{M}_y(x,0,t) = \mathscr{M}_y(x,b,t) = 0\,. \end{aligned} \tag{3.154}$$

The eigenmodes are

$$\Phi_{mn}(x,y) = \sin\frac{m\pi x}{a}\sin\frac{n\pi y}{b}, \tag{3.155}$$

and the wavenumbers take the discrete values:

$$k_{mn}^2 = k_m^2 + k_n^2 = \frac{m^2\pi^2}{a^2} + \frac{n^2\pi^2}{b^2}. \tag{3.156}$$

Using the dispersion equation, the associated angular eigenfrequencies are obtained

$$\omega_{mn} = \pi^2\sqrt{\frac{1}{\rho_p h}}\sqrt{D_1\frac{m^4}{a^4} + D_3\frac{n^4}{b^4} + (D_2+D_4)\frac{m^2n^2}{a^2b^2}}\,. \tag{3.157}$$

In these expressions, m and n are positive integers.[17] As previously shown for strings in Sect. 3.3.2, the eigenmodes Φ_{mn} are orthogonal with respect to mass and stiffness, which means here:

$$\int_0^a\int_0^b \rho_p h\Phi_{mn}(x,y)\Phi_{m'n'}(x,y)dx\,dy = \begin{cases} 0 & \text{if } m\neq m' \text{ or } n\neq n', \\ M_{mn} & \text{if } m=m' \text{ and } n=n'. \end{cases} \tag{3.158}$$

where M_{mn} is the modal mass for the mode (m,n). The eigenfrequencies of the orthotropic plate are distributed in an area located between two limiting dispersion curves (see Fig. 3.34).

3.5.3.2 Isotropic Case

For an isotropic material, one needs to substitute in the previous equations:

$$\begin{aligned} D_1 = D_3 = D = \frac{Eh^3}{12(1-\nu^2)} \text{ and} \\ D_4 = \frac{Eh^3}{6(1+\nu)}\ ;\ D_2 = 2D_1 - D_4 = \frac{E\nu h^3}{6(1-\nu^2)}\,. \end{aligned} \tag{3.159}$$

[17] They can also be zero in case of free boundary conditions.

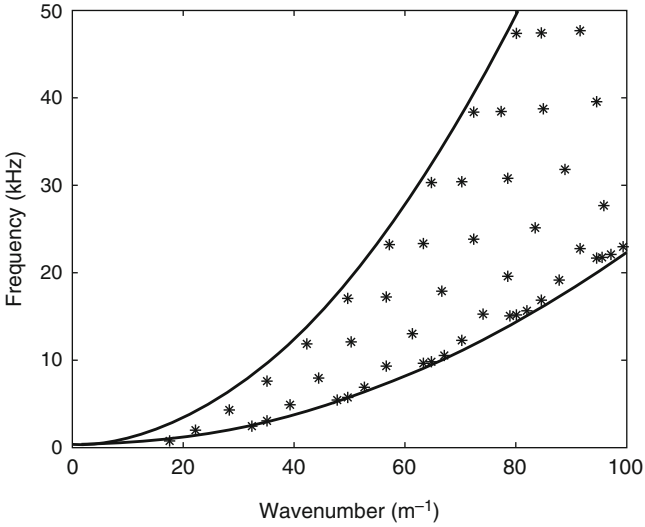

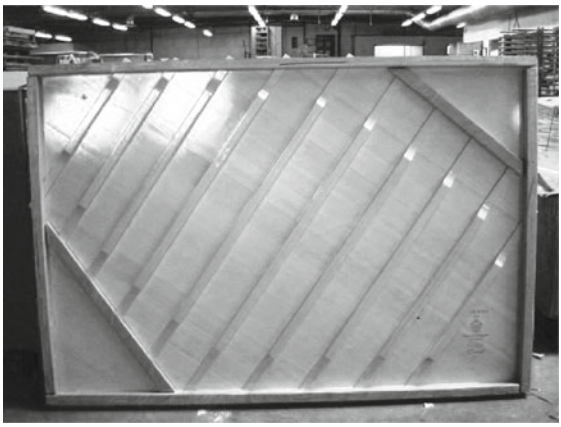

Fig. 3.34 (*Top*) Example of dispersion curves for an orthotropic plate. The eigenfrequencies (*asterisk*) are located between two limiting curves corresponding to the highest and lowest elasticity modulus, respectively. (*Bottom*): The soundboard of an upright piano is an example of an orthotropic plate. The ribs oriented perpendicularly to the fibers increase the transverse stiffness significantly. (© Itemm)

Here, the elastic behavior of the material is entirely determined by two constants: the Young's modulus E and the Poisson's ratio ν. The equation of motion of the plate becomes

$$\rho_p h \frac{\partial^2 W}{\partial t^2} + D\left(\frac{\partial^4 W}{\partial x^4} + 2\frac{\partial^4 W}{\partial x^2 \partial y^2} + \frac{\partial^4 W}{\partial y^4}\right) = 0\,. \tag{3.160}$$

The mode shapes $\Phi_{mn}(x,y)$ have the same form as in Eq. (3.155). However, the eigenfrequencies are now given by:

$$\omega_{mn} = \pi^2 \sqrt{\frac{D}{\rho_p h}} \left[\frac{m^2}{a^2} + \frac{n^2}{b^2} \right] . \tag{3.161}$$

Prestressed Isotropic Plate

For a prestressed plate, under the combined effects of a tension T_x applied in the plane of the plate in the direction Ox and a tension T_y applied along Oy, then the isotropic plate equation is modified in the following way [4]:

$$\rho_p h \frac{\partial^2 W}{\partial t^2} + D \left(\frac{\partial^4 W}{\partial x^4} + 2 \frac{\partial^4 W}{\partial x^2 \partial y^2} + \frac{\partial^2 W}{\partial y^4} \right) - T_x \frac{\partial^2 W}{\partial x^2} - T_y \frac{\partial^2 W}{\partial y^2} = 0 . \tag{3.162}$$

In this case, the eigenfrequencies become

$$\omega_{mn} = \sqrt{\frac{1}{\rho_p h}} \sqrt{D \left(\frac{\pi^2 m^2}{a^2} + \frac{\pi^2 n^2}{b^2} \right)^2 + T_x \frac{m^2 \pi^2}{a^2} + T_y \frac{n^2 \pi^2}{b^2}} . \tag{3.163}$$

3.5.3.3 Modal Density of a Plate

Because of their 2D geometry, plates show higher modal density than bars. As a consequence of damping, especially in wood, a high density of modes leads to a modal overlap (as in membranes), which means that it becomes difficult, or even impossible, to isolate a particular mode.

The case of a simply supported isotropic plate is considered here as an example. Its eigenfrequencies are given by (3.161). Taking the square root of this expression, we obtain $\sqrt{\omega_{mn}} = \sqrt{C} \sqrt{\frac{m^2}{a^2} + \frac{n^2}{b^2}}$, where $C = \pi^2 \sqrt{\frac{D}{\rho_p h}}$. In the k-plane (see Fig. 3.33), the quantity $\sqrt{\omega_{mn}/C}$ is represented by a vector pointing from the origin to the coordinates $(m/a, n/b)$.

As previously done for membranes, the number of modes $N(f)$ contained in the interval $[0, f]$ is calculated. For this purpose, a circle arc of radius $R = \sqrt{\omega/C}$ is drawn in the k-plane. The number of discrete points contained in a quarter of this circle of area $\pi R^2/4 = \frac{\pi \omega}{4C}$ is determined. Since the area of a single rectangular element is $1/ab$, the total number of modes below a given frequency f is given by:

$$N(f) = \frac{ab}{2} \sqrt{\frac{\rho_p h}{D}} f, \tag{3.164}$$

from which we derive the modal density:

$$D(f) = \frac{ab}{2}\sqrt{\frac{\rho_p h}{D}} = \frac{ab}{h}\sqrt{\frac{3\rho_p(1-\nu^2)}{E}}\,. \tag{3.165}$$

In summary, the modal density for a simply supported isotropic plate is constant. This constant is a function of both the geometry and elastic properties of the material. The modal density increases as the plate becomes more flexible, or thinner, and when its surface area increases. For an orthotropic plate whose rigidity constants have the property $D_2+D_4 = 2\sqrt{D_1 D_3}$, we obtain the same expression as Eq. (3.165) for the modal density, provided that D is replaced by D_1 and b by $\beta = b\left(\frac{D_1}{D_3}\right)^{1/4}$. For a given plate geometry and material, orthotropy leads to an increase in the modal density compared to the isotropic case [32].

Particular Case of a Prestressed Isotropic Plate

The influence of prestress on the eigenfrequencies of a plate can be discussed with the help of Eq. (3.163). In this equation, the terms of highest degrees in m and n are modified by the respective factors $1+\frac{T_x}{\pi^2 D}\frac{a^2}{m^2}$ and $1+\frac{T_y}{\pi^2 D}\frac{b^2}{n^2}$. If T_x and T_y are positive (tensile case), the eigenfrequencies increase compared to the non-prestressed case. If T_x and T_y are negative, the overall stiffness decreases, and the eigenfrequencies decrease. The consequences in terms of modal density are not straightforward. The analytical calculation was made by Wilkinson [40] who showed that the effects of prestress are essentially noticeable on the lowest modes, and that the modal density of the prestressed plate tends asymptotically to modal density of a plate without tension as the frequency increases. In addition, the modal density is a function of the squared tension, so that it is independent of its sign. As shown in the PhD manuscript by Ege [17, p. 151], the modal density of a plate decreases with the prestress, whatever its sign. One can also show that the modal density of a plate under high tension becomes close to the modal density of a membrane: this is coherent from a physical point of view.

3.5.3.4 Other Boundary Conditions for Plates

The general determination of eigenmodes for plates under complex boundary conditions will not be discussed in this book. One can refer, for example, to books by Yu [44] and Graff [21] for more information. Only the case of an isotropic rectangular plate is briefly presented below. The standard method used is separation of variables. It involves testing in Eq. (3.160) solutions of the form:

$$w(x,y,t) = X(x)Y(y)e^{j\omega t}\,. \tag{3.166}$$

As a result X and Y must obey:

$$X^{iv}Y + 2X''Y'' + XY^{iv} - \beta^4 XY = 0 \quad \text{with} \quad \beta^4 = \frac{\omega^2 \rho_p h}{D} . \tag{3.167}$$

The variables can be separated under the conditions:

$$\begin{aligned} &Y'' = -\gamma^2 Y \ \text{ and } \ Y^{iv} = \gamma^4 Y \\ &\text{or, alternatively} \\ &X'' = -\alpha^2 X \ \text{ and } \ X^{iv} = \alpha^4 X . \end{aligned} \tag{3.168}$$

In a third case, both conditions can be satisfied simultaneously. In Eq. (3.168), α^2 and γ^2 are real positive numbers given by the boundary conditions. Let us suppose that the conditions of the second group (those relating to X) are satisfied. We then derive from Eq. (3.167) the condition for Y, for each value α_n of α defined by the boundary conditions on X:

$$Y^{iv} - 2\alpha_n^2 Y'' - (\beta^4 - \alpha_n^4) Y = 0 . \tag{3.169}$$

Equation (3.169) has different types of solution, depending on the value of β compared to α. For $\beta > \alpha$, we get

$$\begin{aligned} &Y(y) = A \sin k_2 y + B \cos k_2 y + C \sinh k_1 y + D \cosh k_1 y \\ &\text{with} \quad k_1 = \sqrt{\beta^2 + \alpha_n^2} \quad \text{and} \quad k_2 = \sqrt{\beta^2 - \alpha_n^2} . \end{aligned} \tag{3.170}$$

The constants A, B, C, and D are then determined by the boundary conditions in y. For a plate clamped at $y = 0$ and $y = b$, for example, we have the conditions:

$$Y(0) = Y'(0) = Y(b) = Y'(b) = 0 . \tag{3.171}$$

The eigenfrequencies are given by the roots of the determinant of the system of equations that governs the constants, which yields

$$k_1 k_2 \left[\cos k_2 b \cosh k_1 b - 1\right] - \alpha_n^2 \sin k_2 b \sinh k_1 b = 0 . \tag{3.172}$$

For each value of n, Eq. (3.172) provides the m successive values of β (and, in turn, the eigenfrequencies ω). The same equations can then be used to calculate the eigenshape associated with each mode.

3.5.3.5 Piano Soundboard and Ribbed Structures

Ribbed plates and shells can be found in numerous vehicles (planes and ships) and in architecture. The prime function of ribs is to increase the rigidity of a given structure without increasing its mass too much. In Chap. 13, it will be shown that such a property also is desirable for enhancing the radiation efficiency of stringed instruments. For this reason, guitar and piano soundboards, for example, are reinforced by ribs (see Fig. 3.34). Another reason follows from static considerations. As mentioned in Chap. 1, wood is an orthotropic material. As a consequence, wooden plates are more rigid in the direction of the fibers than in the direction perpendicular to them, where they can break more easily. Therefore, if the purpose is to globally stiffen the soundboard, for dynamical and acoustical reasons, as well as to increase its breaking strength, then a good strategy consists is to glue the ribs perpendicular to the fibers.

In the case of the piano, the soundboard is also stiffened by the bridges, which are fixed on the upper side, where the strings are attached (see Fig. 1.1 in Chap. 1). The combination of the ribs and bridges has pronounced effects on the sound quality of a piano, as underlined by several studies and patents in the past decades [6, 14]. The exact nature of these effects was identified and quantified more accurately in recent studies [8, 13]. Let us consider, first, the simplified example of a ribbed plate whose geometry and material are comparable to those of an upright piano soundboard. As long as the modal frequencies remain lower than, say, 1 kHz, then the way the ribs are spaced has little effect on the global patterns of the modal shapes (see Fig. 3.35).

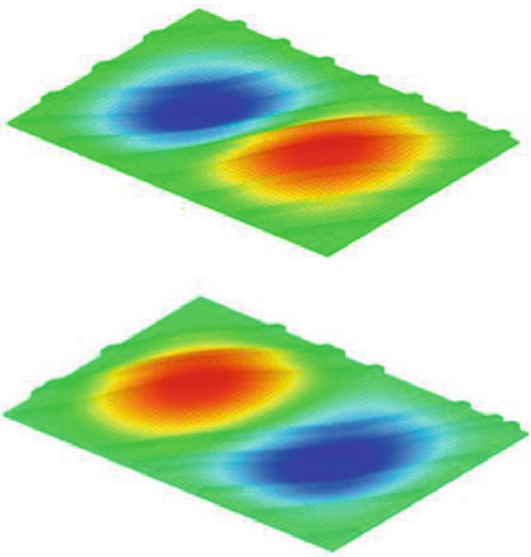

Fig. 3.35 Influence of the ribs on the modal shapes of the lowest modes of a ribbed soundboard. (*Top*) Regularly spaced ribs; (*Bottom*) Irregularly spaced ribs

For such an example, one can prove mathematically, with the help of homogenization techniques, that an equivalent homogeneous plate can be defined in this frequency range, with similar properties to the ribbed plate [5]. However, above a certain cutoff frequency (which is near 1.1–1.2 kHz for most upright pianos), the elastic half wavelength becomes of the same order of magnitude as the mean inter-rib distance. As a consequence, the soundboard zones between the ribs behave like "waveguides" bounded by the ribs, as seen on the modal shapes (see Fig. 3.36). At this stage, it is worth noting that the rib distance usually varies slightly on a soundboard. The calculation of the modes then shows that, even for slightly irregular rib spacing, the parts of the soundboard with significant amplitudes are restricted to a few inter-ribs zones only (see Fig. 3.36). This is the so-called localization of modes. Such localization effects resulting from small departures from exact periodicity are frequently encountered in physics. They have been intensively studied by Anderson [2]. These phenomena are often referred to as "Anderson's localization effects." On a piano soundboard, the localization is further enhanced by the presence of the bridges. As shown in Fig. 3.36d, only a section of one inter-rib spacing, situated in the region above the main bridge, vibrates significantly. For the frequency shown here (2149 Hz), the bridge appears to act as a supplementary boundary condition. Thus, the vibrational energy is confined in a section of one inter-rib zone

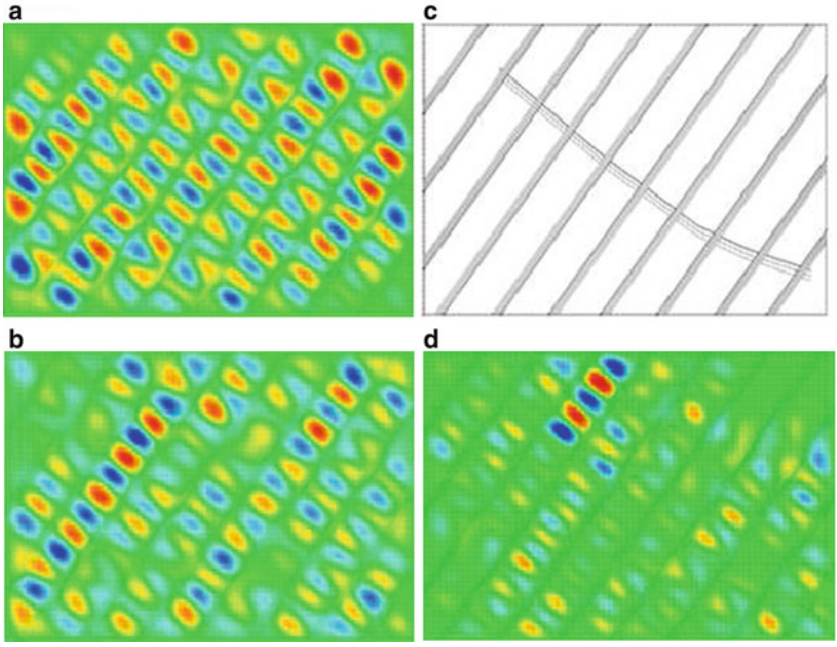

Fig. 3.36 Influence of rib spacing and bridge on the localization of modes for an upright piano soundboard. (**a**) Regular rib spacing; (**b**) Slightly irregular rib spacing; (**c**) Sketch of soundboard with bridge and ribs; (**d**) Increased localization of modes due to the bridge

only. It will be seen in Chap. 7 that the phenomenon is slightly different for wind instruments. Finally, in Chap. 14, the effects of mode localization on piano radiation and, particularly, on the directivity of the radiated field, will be presented.

3.5.4 Vibrations of Shells

As indicated for plates, a detailed study of the vibrations of shells is beyond the scope of this book. The interested reader will find more information in specialized books, such as [35].

3.5.4.1 Spherical Caps

In this section, the vibrations of a thin and shallow spherical cap are investigated. This structure illustrates the effect of a finite radius of curvature, compared with the case of thin circular plates. To a first approximation, it can be assumed that some percussion instruments, such as cymbals and gongs, can be modeled by such shells. We consider here that the vibrations are linear, so that we can use a modal approach. As a consequence, the presentation is restricted to the case of low stress, low strain, and small displacements compared with the shell thickness. As the displacement field of the shell becomes comparable or larger than the shell thickness, nonlinear vibrations will have to be considered, as developed in Chap. 8. In order to account for cymbals and gongs, the particular case of free boundary conditions is treated below. This problem is not commonly addressed in the literature [25].

We consider a spherical cap of thickness h, radius of curvature R, and whose plane projection is a circle of radius a (see Fig. 3.37). The hypotheses of Donnell–Mushtari–Vlasov (see Chap. 1) applied to the case of a thin ($h \ll a$) and shallow ($a \ll R$) shell yield the equation describing the free transverse bending motion $w(r, \theta, t)$ of the cap [35]:

$$D\nabla^4 w + \frac{Eh}{R^2} w + \rho h \ddot{w} = 0 \,, \tag{3.173}$$

where E is the Young's modulus, ρ the density, ν the Poisson's ratio, and $D = \frac{Eh^3}{12(1-\nu^2)}$ the rigidity factor. Equation (3.173) is equivalent to Eq. (1.88) shown in Chap. 1, but with the force function F removed. It is convenient to express this equation in a dimensionless form, through introduction of the reduced variables $\overline{w} = w/w_o$, $\overline{r} = r/a$ and $\overline{t} = t/t_o$ with $t_o = a^2\sqrt{\frac{\rho h}{D}}$. We get

$$\nabla^4 \overline{w} + \chi \overline{w} + \ddot{\overline{w}} = 0 \;\text{ where }\; \chi = 12(1-\nu^2)\frac{a^4}{R^2 h^2} \,. \tag{3.174}$$

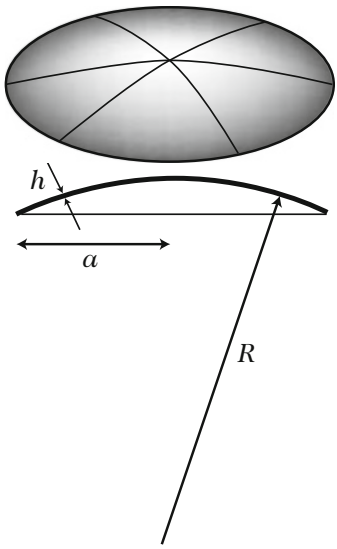

Fig. 3.37 A thin shallow spherical cap. R is the radius of curvature, a is the radius of the circle obtained by projection of the cap on a plane, and h is the thickness. The assumption of *thin* shell means $h \ll a$, and a *shallow* shell is such that $a \ll R$

Note 1: In the linear case, w_o can be chosen arbitrarily. This will not be the case for nonlinear vibrations, as seen in Chap. 8.
Note 2: In what follows, only the dimensionless equation is solved, but the overlines on the variables are omitted, for the sake of clarity.

3.5.4.2 Eigenmodes of a Spherical Cap with Free Edges

We look for solutions of Eq. (3.174) of the form $w(r,\theta,t) = \Phi(r,\theta)q(t)$. These solutions must satisfy one of the following conditions [23]:

$$\begin{cases} \text{If } \omega^2 - \chi = \zeta^4 > 0 \quad \text{then } \left[\nabla^4 - \zeta^4\right]\Phi = 0 \quad \textbf{case 1} \\ \text{If } \omega^2 - \chi = -\zeta^4 < 0 \text{ then } \left[\nabla^4 + \zeta^4\right]\Phi = 0 \quad \textbf{case 2} \end{cases} \tag{3.175}$$

In **case 1**, the eigenfunctions are given by:

$$\Phi_{nm}(r,\theta) = \left[A_n r^n + B_n J_n(\zeta_{nm} r) + C_n I_n(\zeta_{nm} r)\right] \begin{vmatrix} \cos m\theta \\ \sin m\theta \end{vmatrix} . \tag{3.176}$$

where A_n, B_n, and C_n are constants, ζ_{nm} are determined by the boundary conditions, J_n are the Bessel functions of the first kind, and I_n are the modified Bessel functions of the first kind [1].

In **case 2**, the eigenfunctions are given by:

$$\Phi_{nm}(r,\theta) = \left[A_n r^n + B_n \mathrm{ber}_n(\zeta_{nm} r) + C_n \mathrm{bei}_n(\zeta_{nm} r)\right] \begin{vmatrix} \cos m\theta \\ \sin m\theta \end{vmatrix} . \tag{3.177}$$

where ber_n and bei_n are the Kelvin's functions defined by [1]:

$$\mathrm{ber}_n(x) + j\mathrm{bei}_n(x) = J_n(x \exp(3j\pi/4)) \,. \tag{3.178}$$

For a free edge, the eigenvalues ζ_{mn} are determined by the boundary conditions (1.94) at $r = a$. Four different situations may occur [36]:

$$\begin{cases} \text{for } n \in \{0,1\}, \quad \forall m \geq 1 \quad \omega_{nm} = \sqrt{\chi + \omega_{nm}^{(0)2}} \\ \text{for } n \geq 2, \quad m = 0 \quad \text{and } \chi < \chi_n^{\lim} \quad \omega_{n0} = \sqrt{\chi + \zeta_{n0}^4} \\ \text{for } n \geq 2, \quad m = 0 \quad \text{and } \chi > \chi_n^{\lim} \quad \omega_{n0} = \sqrt{\chi - \zeta_{n0}^4} \\ \text{for } n \geq 2, \quad m \geq 1, \quad \omega_{nm} = \sqrt{\chi + \zeta_{nm}^4} \end{cases} \tag{3.179}$$

where $\omega_{nm}^{(0)}$ are the eigenfrequencies of a circular plate with free edges of radius a, corresponding to the limiting case of a cap with zero curvature (infinite radius of curvature). Figure 3.38 shows how the different eigenfrequencies of the cap vary as a function of the curvature parameter χ.

The limiting value of the parameter χ that makes the difference between "Bessel" modes and axisymmetric "Kelvin" modes is given by Johnson and Reissner [23]:

$$\chi_n^{\lim} = \frac{(1-\nu)(3+\nu)n^2(n^2-1)}{1 + \frac{1}{4}(1-\nu)(n-2) - \frac{n^2(n-1)(1-\nu)(4n-\nu+9)}{16(n+2)^2(n+3)}} \,. \tag{3.180}$$

Appendix: Modal Decomposition Using the Residue Calculus

One often needs to expand a transfer function $G(\omega)$ in the frequency domain onto a modal basis. In this case residue calculus is a powerful tool. It yields, in turn, the inverse Fourier transform $g(t)$ as a sum of damped sinusoids. We restrict ourselves to the simple, though frequently encountered, case where the poles of the function $G(\omega)$ are simple. These poles ω_n are generally complex. It is assumed here that their imaginary part is positive, so that the function $\exp(j\omega_n t)$ is decreasing for $t > 0$. The poles are therefore located in the upper complex half-plane. The result, shown below, is the following:

$$g(t) = j \sum_n R_n e^{j\omega_n t} \quad \text{for } t > 0, \tag{3.181}$$

with $g(t) = 0$ for $t < 0$. The quantities R_n are the residues defined for simple poles by:

$$R_n = \lim_{\omega \longrightarrow \omega_n} (\omega - \omega_n) G(\omega). \tag{3.182}$$

(continued)

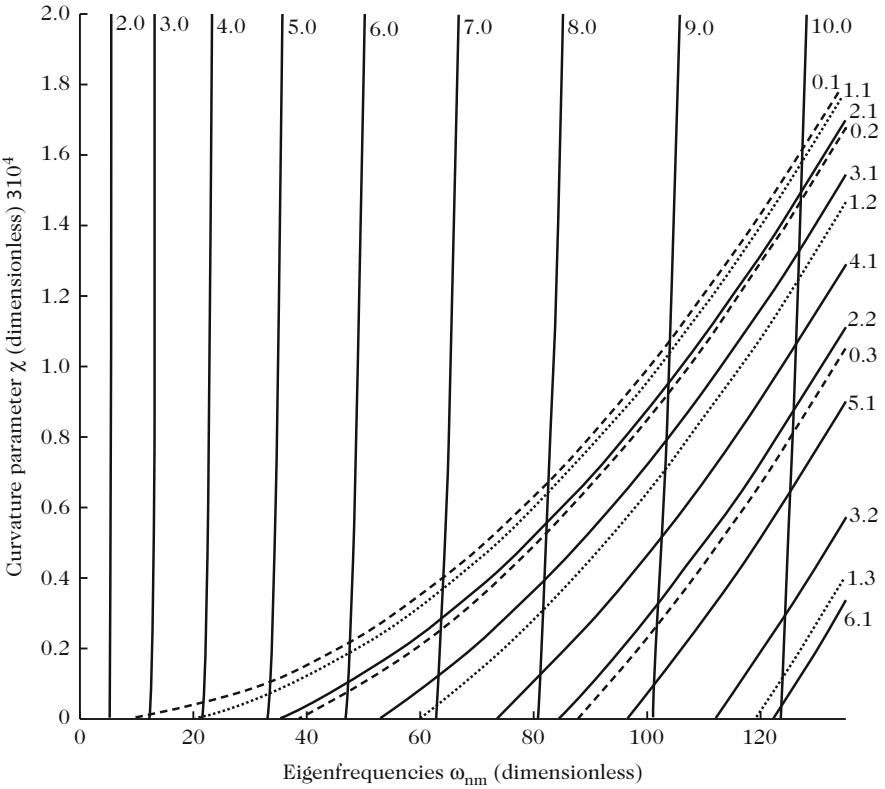

Fig. 3.38 Variations of the eigenfrequencies for a spherical cap with curvature parameter χ. Notice that the eigenfrequencies increase with χ, except for the modes ω_{n0} which remain almost unchanged

If $G(\omega) = N(\omega)/D(\omega)$, in order to calculate the residues, one only needs to write the denominator in the form[18] $D(\omega) \simeq (\omega - \omega_n)D'(\omega_n)$. As a consequence, we get

$$R_n = \frac{N(\omega_n)}{D'(\omega_n)}. \tag{3.183}$$

For the proof, we start from the definition of $g(t)$ [see Eq. (1.116)] :

$$g(t) = \frac{1}{2\pi}\int_{-\infty}^{+\infty} G(\omega)e^{j\omega t}d\omega. \tag{3.184}$$

(continued)

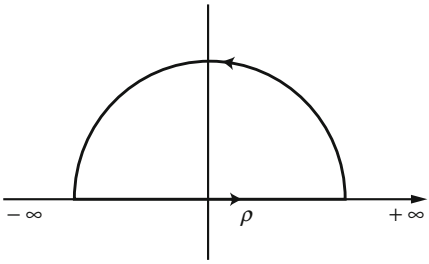

Fig. 3.39 Contour of the integral (3.185), equivalent to the integral on the real axis. The equivalence applies when the radius of the circle ρ tends to infinity, since the function to integrate on the circle tends to 0

The integration is carried out for a real ω, from $-\infty$ to $+\infty$, but we can convert it to a contour integral: as a consequence the integral on the contour presented in Fig. 3.39 is equal to the integral (3.184), when $t > 0$. The coordinate of a point located on the semi-circle of the complex plane can be written: $z = \rho\cos\theta + j\rho\sin\theta$, with $\sin\theta > 0$. When t is positive, and when the radius ρ of the circle tends to infinity, the quantity $G(z)e^{jzt}$ tends to 0, provided that the modulus of the function $G(z)$ tends sufficiently quickly to 0 as z tends to infinity (Jordan's lemma). The value of the contour integral on the semi-circle tends to 0, and this contour integral is the result that we were searching for.

The residue theorem states

$$\oint F(z)dz = 2\pi j \sum \text{Residues}(F(z)). \tag{3.185}$$

In this formula, the contour goes counterclockwise. We obtain

$$g(t) = j\sum \text{Residues}(G(\omega)e^{j\omega t}) = j\sum_n R_n e^{j\omega_n t}.$$

For $t < 0$, we can use the symmetrical contour with regard to the real axis. This contour is located in the lower half-plane, and since there are no poles in this half-plane, it is equal to 0. Given the choice made for the poles of $G(\omega)$, we find that $g(t)$ is causal.

In addition, since the function $g(t)$ is real, the poles are grouped by pairs: the existence of terms of the form $jR_n\exp(j\omega_n t)$ implies terms $-jR_n^*\exp(-j\omega_n^* t)$. Similarly, the existence of poles ω_n implies the poles $-\omega_n^*$ (which are also located in the upper half-plane).

Finally, taking the Fourier transform of (3.181) yields

$$G(\omega) = \sum_n \frac{R_n}{\omega - \omega_n} = \sum_n \frac{N(\omega_n)}{(\omega - \omega_n)D'(\omega_n)}. \tag{3.186}$$

(continued)

To prove this, we can apply the formula (3.181) to the function $R_n/(\omega - \omega_n)$, whose residue is R_n! When ω tends towards ω_n, only the nth-term of the series is relevant, since we have: $G(\omega) = N(\omega_n)/\left[(\omega - \omega_n)D'(\omega_n)\right] = N(\omega)/D(\omega)$.

A difficulty remains for the poles located on the real axis: the formula given for the poles located in the upper half-plane is valid, but the proof is more difficult (it uses the necessary causality of the function $g(t)$).

References

1. Abramowitz, M., Stegun, I.A.: Handbook of Mathematical Functions, with Formulas, Graphs, and Mathematical Tables. Dover, New York (1972)
2. Anderson, P.: Absence of diffusion in certain random lattices. Phys. Rev. **109**, 1492–1505 (1958)
3. Askenfelt, A., Jansson, E.V.: From touch to string vibrations. III: String motion and spectra. J. Acoust. Soc. Am. **93**(4), 2181–2196 (1993)
4. Axisa, F., Trompette, P.: Modelling of Mechanical Systems: Structural Elements. Elsevier, Oxford (2005)
5. Berthaut, J., Ichchou, M., Jézéquel, L.: Piano soundboard: structural behavior, numerical and experimental study in the modal range. Appl. Acoust. **64**, 1113–1136 (2003)
6. Bilhuber, P.H., Johnson, C.A.: The influence of the soundboard on piano tone quality. J. Acoust. Soc. Am. **11**(3), 311–320 (1940)
7. Boutillon, X.: Model for piano hammers: experimental determination and digital simulation. J. Acoust. Soc. Am. **83**(2), 746–754 (1988)
8. Boutillon, X., Ege, K.: Vibroacoustics of the piano soundboard: reduced models, mobility synthesis, and acoustical radiation regime. J. Sound Vib. **332**(18), 4261–4279 (2013)
9. Boutillon, X., Weinreich, G.: Three-dimensional mechanical admittance: theory and new measurement method applied to the violin bridge. J. Acoust. Soc. Am. **105**(6), 3524–3533 (1999)
10. Chaigne, A., Askenfelt, A.: Numerical simulations of piano strings. I. A physical model for a struck string using finite difference methods. J. Acoust. Soc. Am. **95**(2), 1112–1118 (1994)
11. Chaigne, A., Askenfelt, A.: Numerical simulations of piano strings. II. Comparisons with measurements and systematic exploration of some hammer-string parameters. J. Acoust. Soc. Am. **95**(3), 1631–1640 (1994)
12. Chaigne, A., Doutaut, V.: Designing and building a xylophone prototype (in French). Research report, ENST (1997)
13. Chaigne, A., Cotté, B., Viggiano, R.: Dynamical properties of piano soundboards. J. Acoust. Soc. Am. **133**(4), 2456–2466 (2013)
14. Conklin, H.A.: Soundboard construction for stringed musical instruments. US Patent 3866506 (1975)
15. Courant, R., Hilbert, D.: Methods of Mathematical Physics, vol. 1. Interscience Publishers, New York (1966)
16. Dautray, R., Lions, J.: Mathematical analysis and numerical methods for science and technology. In: Evolution Problems II, vol. 6. Springer, Berlin (2000)
17. Ege, K.: The piano soundboard: modal studies in the low- and mid-frequency range (in French). Ph.D. thesis, Ecole polytechnique, Palaiseau (2009)
18. Géradin, M., Rixen, D.: Mechanical Vibrations: Theory and Application to Structural Dynamics. Wiley, Chichester (1999)

19. Gibert, R.J.: Vibrations of Structures. Interaction with Fluids. Random Excitation Sources (in French). Eyrolles, Paris (1988)
20. Gillan, F.S., Elliott, S.J.: Measurement of the torsional modes of vibration of strings on instruments of the violin family. J. Sound Vib. **130**(2), 347–351 (1989)
21. Graff, K.F.: Wave Motion in Elastics Solids. Dover, New York (1991)
22. Hall, D.E.: Piano string excitation. VI: Nonlinear modeling. J. Acoust. Soc. Am. **92**(1), 95–105 (1992)
23. Johnson, M.W., Reissner, E.: On transverse vibrations of spherical shells. Q. Appl. Math. **15(4)**, 367–380 (1956)
24. Le Carrou, J.L.: Vibro-acoustics of the concert harp. Ph.D. thesis, Ecole doctorale de l'Université du Maine, Le Mans (2006). http://tel.archives-ouvertes.fr/
25. Liew, K.M., Lim, C.W., Kitipornchai, S.: Vibrations of shallow shells: a review with bibliography. Trans. ASME Appl. Mech. Rev. **8**, 431–444 (1997)
26. Meirovitch, L.: Fundamentals of Vibrations. McGraw-Hill, New York (2001)
27. Morse, P.M., Ingard, K.: Theoretical Acoustics. McGraw-Hill, New York (1968)
28. Orduna-Bustamante, F.: Nonuniform beams with harmonically related overtones for use in percussion instruments. J. Acoust. Soc. Am. **90**(6), 2935–2941 (1991)
29. Pickering, N.: Problems in string making. J. Catgut Acoust. Soc. **2**(3), 1–4 (1993)
30. Podlesak, M., Lee, A.R.: Dispersion of waves in piano strings. J. Acoust. Soc. Am. **83**(1), 305–317 (1988)
31. Politzer, D.: Banjo timbre from string stretching and frequency modulation. Acta Acust. United Acust. **101**(1), 1–4 (2015)
32. Renji, K., Nair, P., Narayanan, S.: Modal density of composite honeycomb sandwich panels. J. Sound Vib. **195**(5), 687–699 (1996)
33. Rossing, T.D.: Science of Percussion Instruments. World Scientific, Singapore (2000)
34. Schumacher, R.: Measurements of some parameters of bowing. J. Acoust. Soc. Am. **96**(4), 1985–1998 (1994)
35. Soedel, W.: Vibrations of Shells and Plates, 3rd edn. Marcel Dekker Inc., New York (2004)
36. Thomas, O., Touzé, C., Chaigne, A.: Non-linear vibrations of free-edge thin spherical shells: modal interaction rules and 1:1:2 internal resonance. Int. J. Solid Struct. **42**(1), 3339–3373 (2005)
37. Trautmann, L., Rabenstein, R.: Digital Sound Synthesis by Physical Modeling Using the Functional Transformation Method. Kluwer, New York (2003)
38. Valette, C., Cuesta, C.: Mechanics of the Vibrating String (in French). Hermès, Paris (1993)
39. Weinreich, G.: Coupled piano strings. J. Acoust. Soc. Am. **62**, 1474–1484 (1977)
40. Wilkinson, J.P.D.: Modal densities of certain shallow structural elements. J. Acoust. Soc. Am. **43**(2), 245–251 (1968)
41. Wolfe, J.: Music acoustics web page, the University of New South Wales. http://www.phys.unsw.edu.au/music/ (2007)
42. Woodhouse, J., Loach, A.: Torsional behaviour of cello strings. Acust. Acta Acust. **85**(5), 734–740 (1999)
43. Worland, R.: Chladni patterns on drumheads: a "physics of music" experiment. Phys. Teach. **49**(1), 24–27 (2011)
44. Yu, Y.Y.: Vibrations of Elastic Plates. Springer, New York (1996)